Microsegregation

Partition coeff.

k=Cs/CL at constant temp. and press.

- if mL < 0 k < 1
- İf mL > 0 k >1

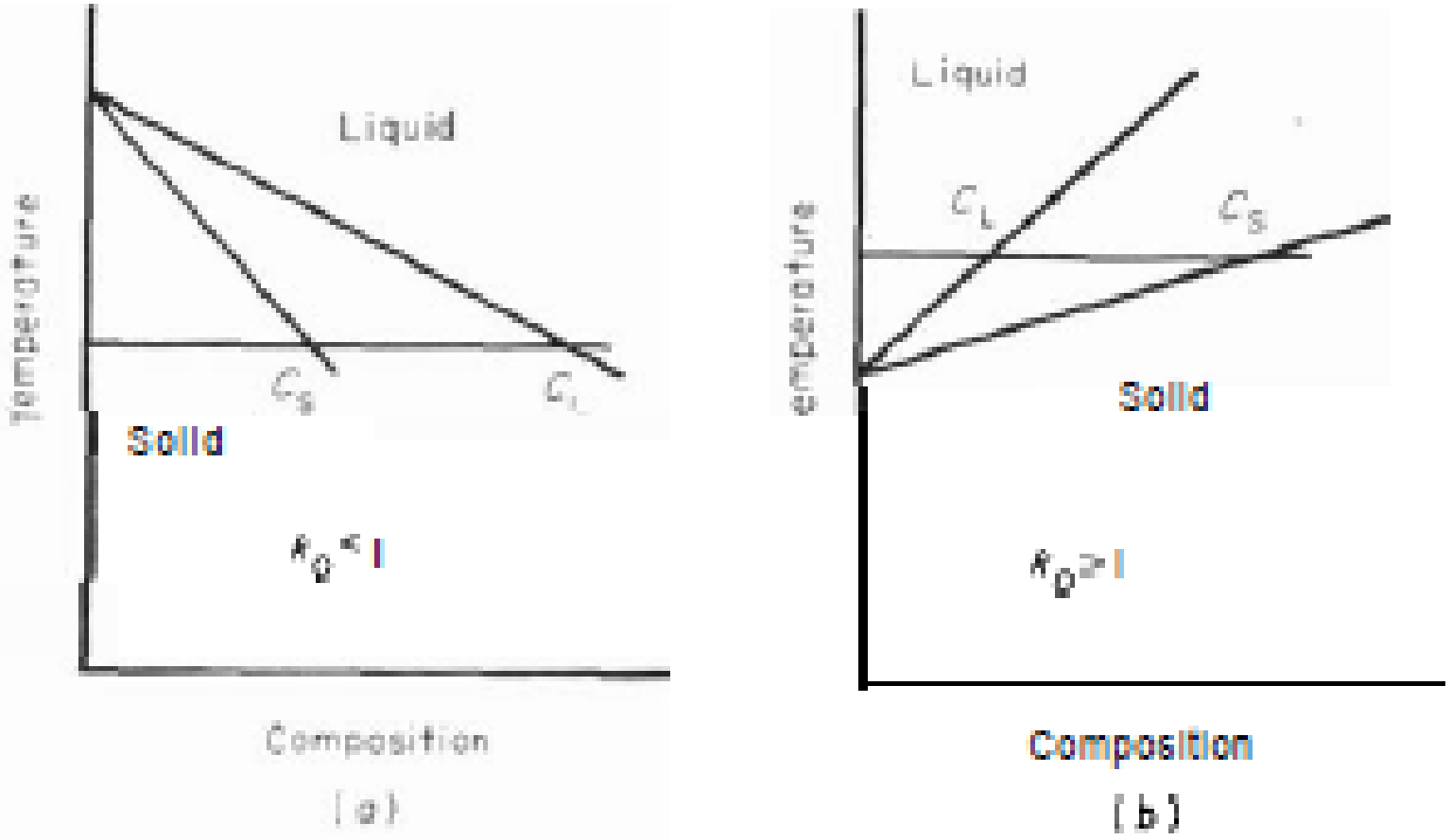

Fig. 4.1 (a) Portion of a phase diagram in which the distribution coefficient $k_0 < 1$. *(b) Portion of a phase diagram in which the distribution coefficient* $k_0 > 1$.

Introduction

Microsegregation is a distribution of solute elements in dendritic or cellular cast structures and can affect mechanical and chemical properties and phase transformations in alloys, such as homogenization and solution heat treatments, pearlite-ferrite banding structure, martensitic transformation and corrosion.

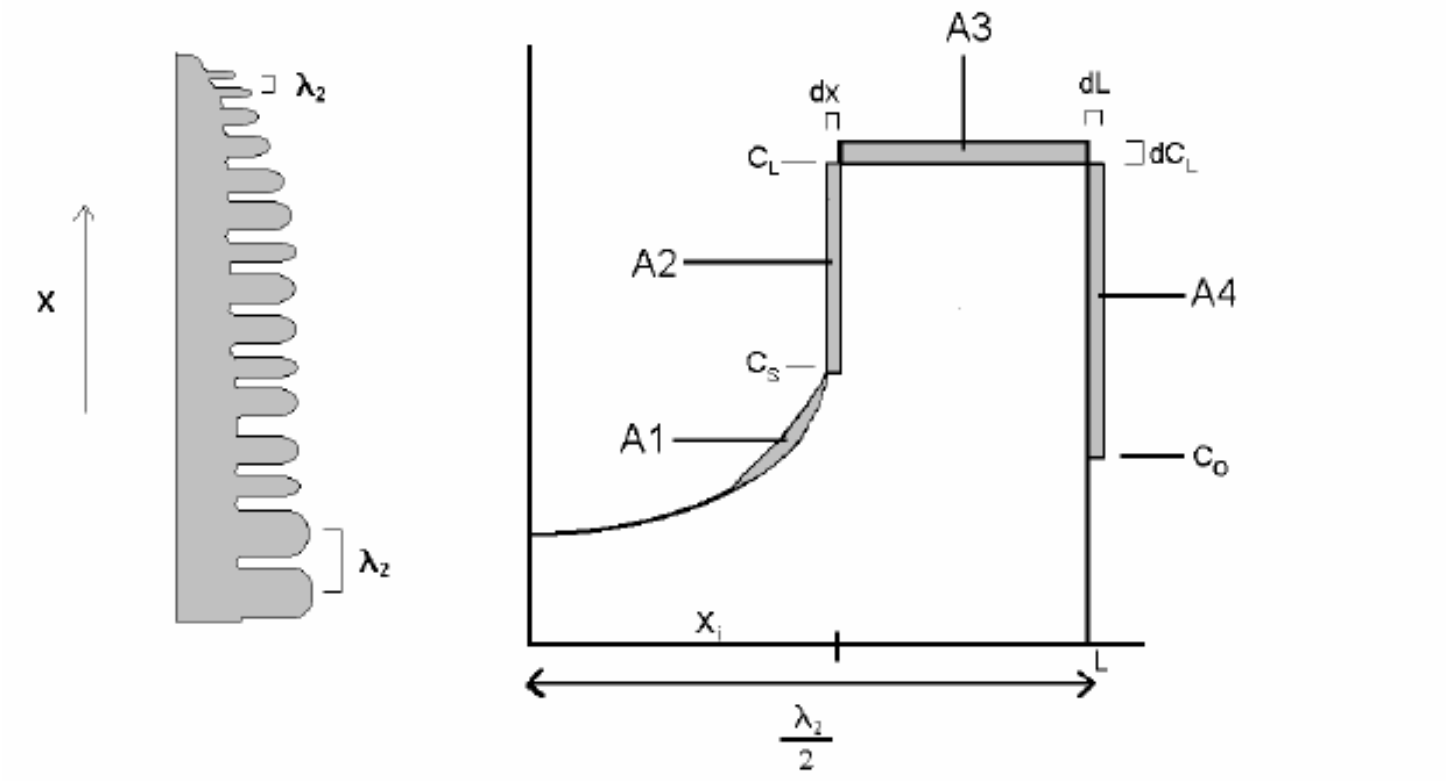

Figure 1 Dimensional form of microsegregation volume element from the centre of side arm to the centre of the liquid pool

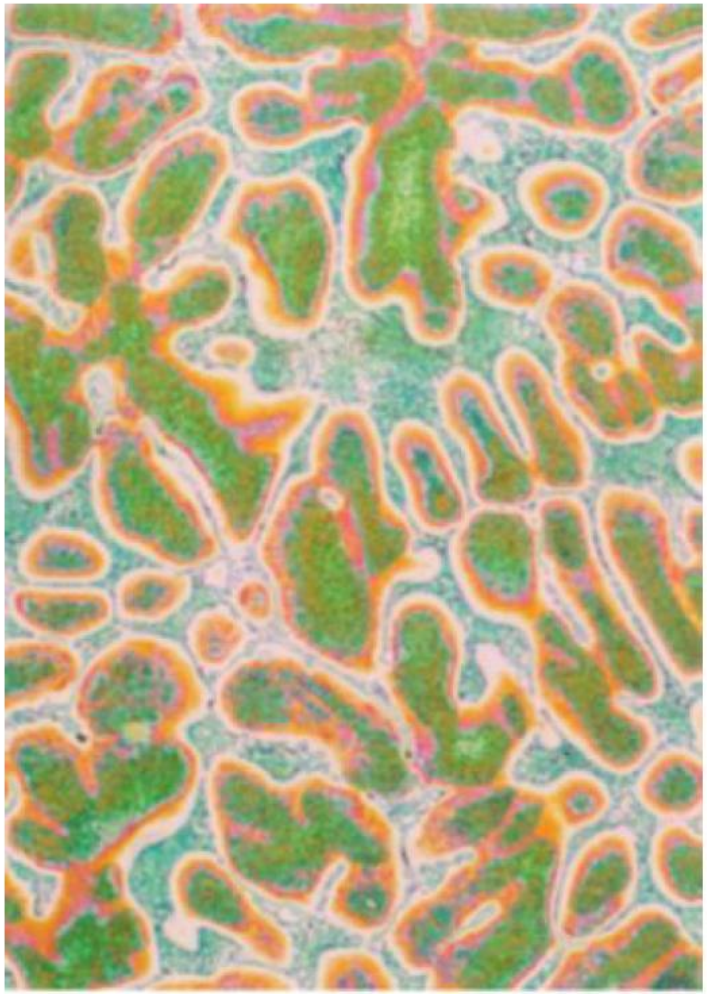

Fig. 37 Phase constituent identification in alloy 356.0 with reagent 13m (Table 4). Time of attack: 5 s. Orange-green fields are primary dendritic microsegregation regions with α-Al (solid solution). Blue fields are interdendritic eutectic (α-Al + Si). 800×. Compare with Table 18. (Małgorzata Warmuzek, Foundry Research Institute, Kraków, Poland)

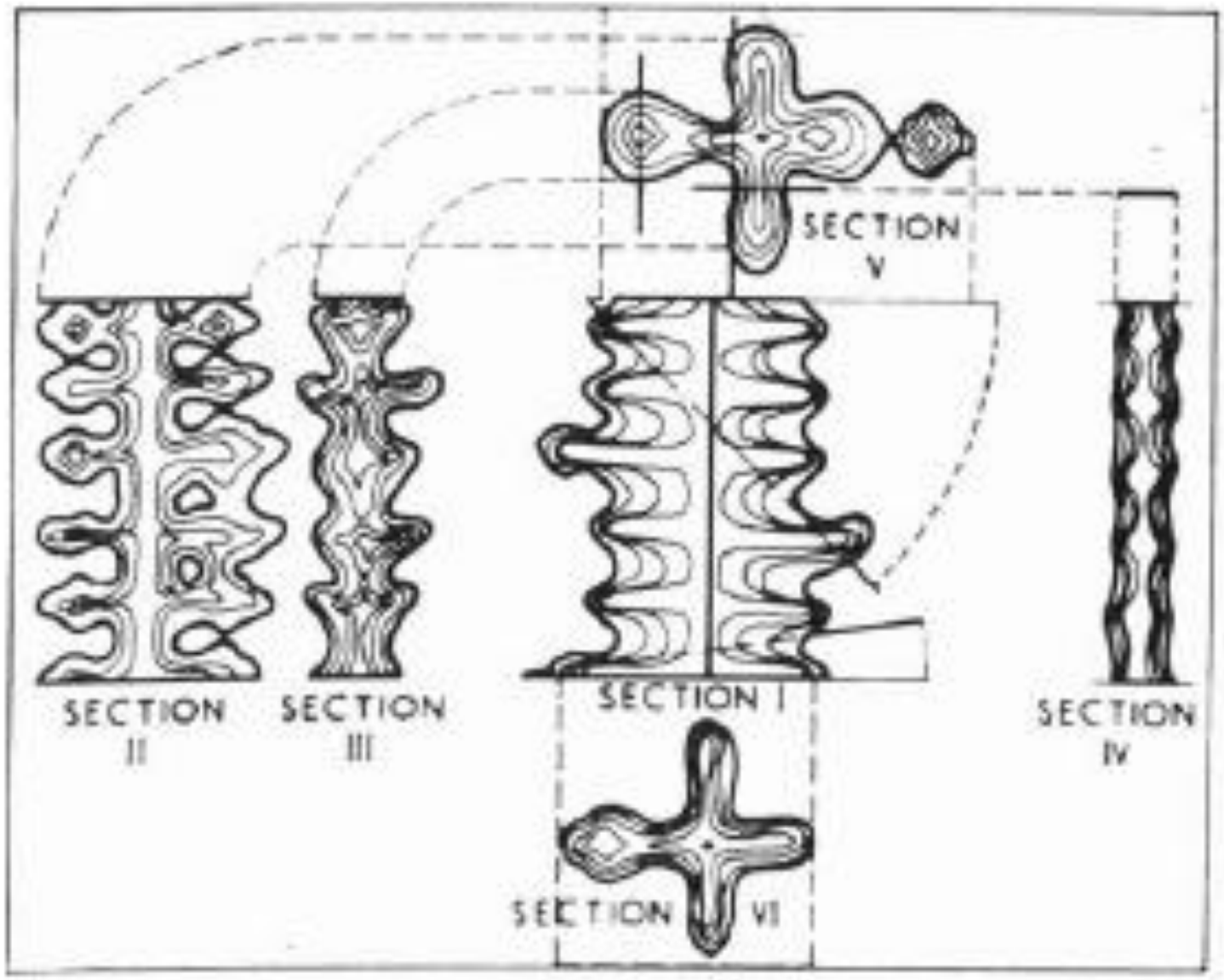

Fig. 7.3 *Isoconcentration surfaces in a columnar dendrite grown in a low-alloy steel melt (Kattamis and Flemings[9]).*

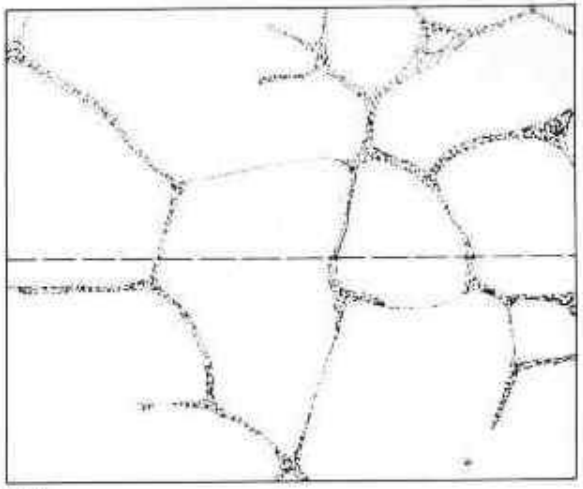

(a)

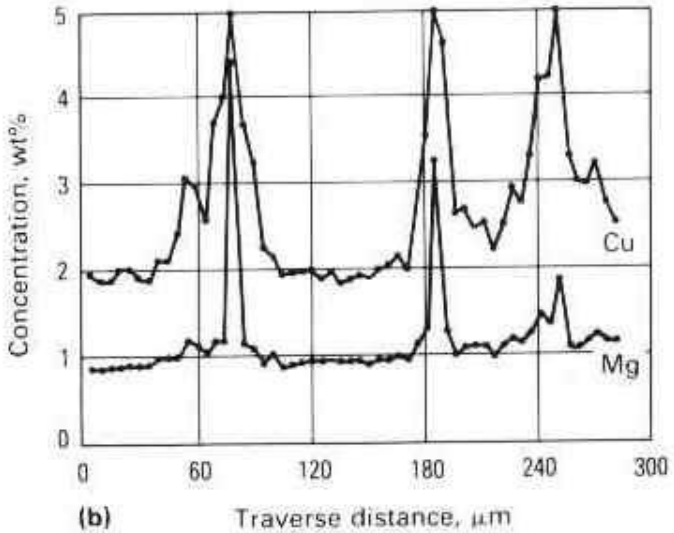

(b)

Fig. 16 Copper and magnesium microsegregation in a direct-chill semicontinuous cast (610 × 1372 mm, or 24 × 54 in.) 2124 alloy ingot. (a) Dendrite cells at midthickness location in ingot and enrichment of copper and magnesium at the cell boundaries. When observed in conjunction with the electron probe microanalysis, the gradual increase in solute concentration across the dendrite cell is readily apparent. (b) Microprobe traverse across dendrites

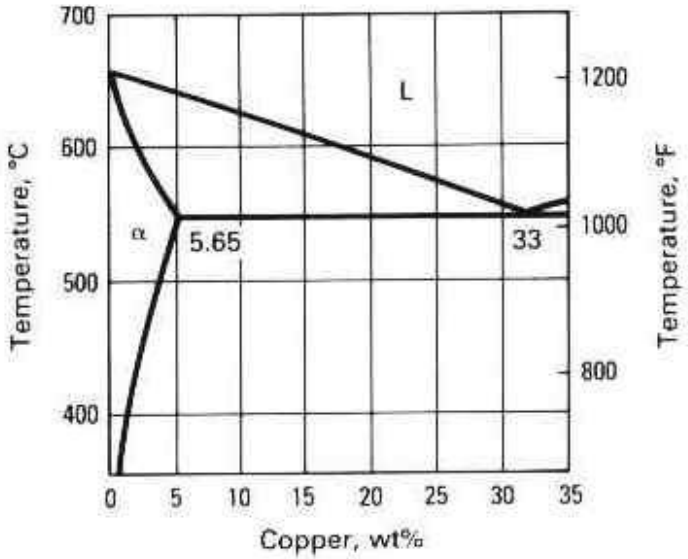

(a)

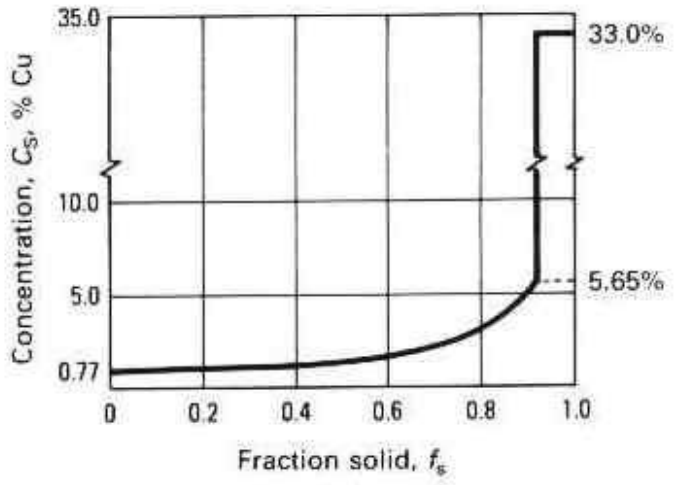

(b)

Fig. 17 (a) The aluminum-rich end of the aluminum-copper phase diagram. (b) Solid composition (C_S) versus fraction solid (f_s) for Al-4.5Cu. L, liquid; α, aluminum solid solution. (Ref 3)

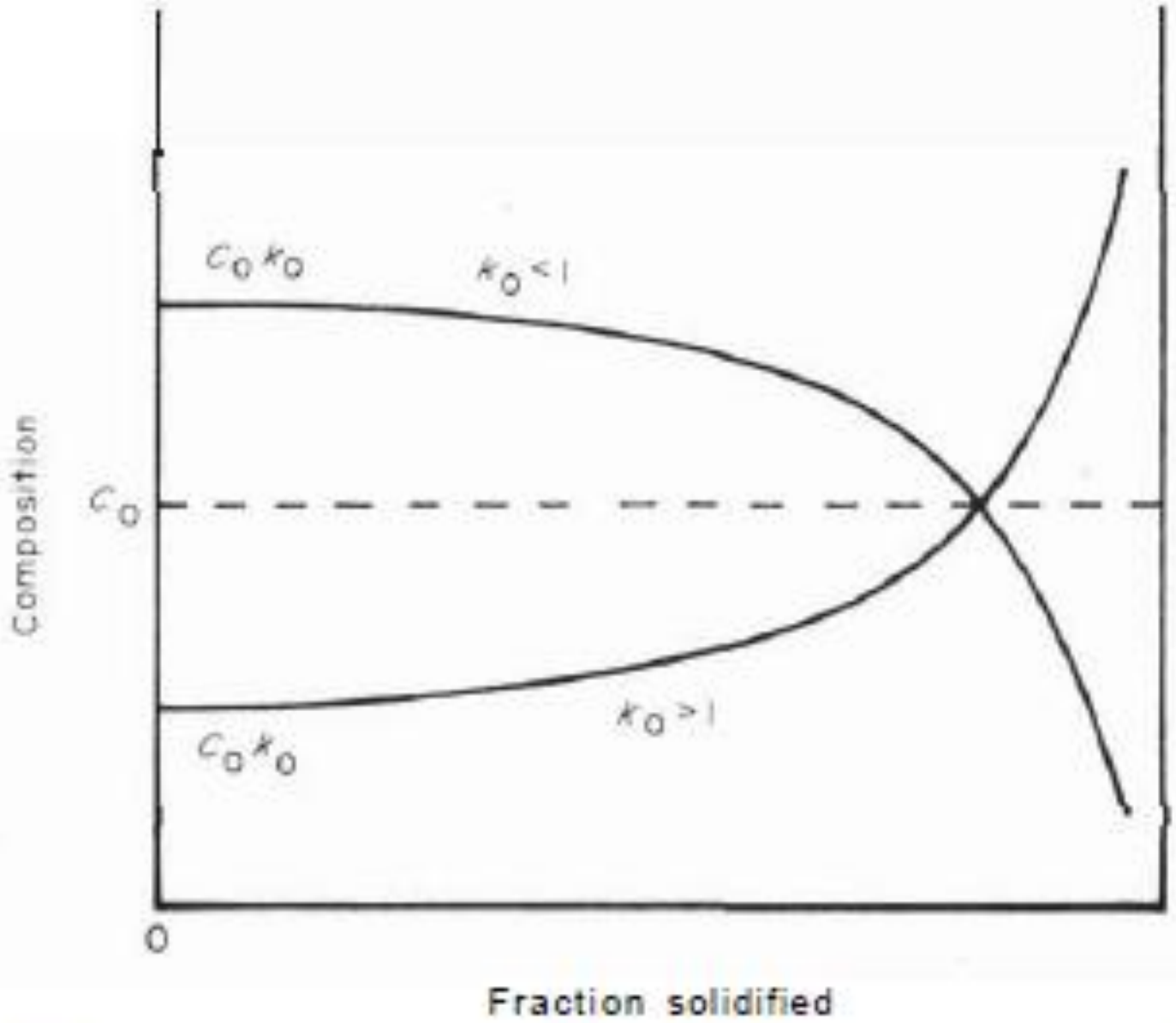

Fig. 4.11 Concentration–distance profiles for a bar solidified under conditions of complete solute mixing in the liquid.

Models for Microsegregation

- 1 no mixing in liquid no diffusion in solid no coarsening
- 2. partial mixing in liquid no diffusion in solid no coarsening
- 3. complete mixing in liquid no diffusion in solid no coarsening
- 4. complete mixing in liquid diffusion in solid no coarsening
- 5. complete mixing in liquid diffusion in solid coarsening
- 6. complete mixing in liquid complete diffusion in solid

- 1 no mixing in liquid no diffusion in solid no coarsening
- 2. partial mixing in liquid no diffusion in solid no coarsening
- 3. complete mixing in liquid no diffusion in solid no coarsening
- 4. complete mixing in liquid diffusion in solid no coarsening
- 5. complete mixing in liquid diffusion in solid coarsening
- **6. complete mixing in liquid complete diffusion in solid**

(6 Model). Eq solidification (Level Rule)

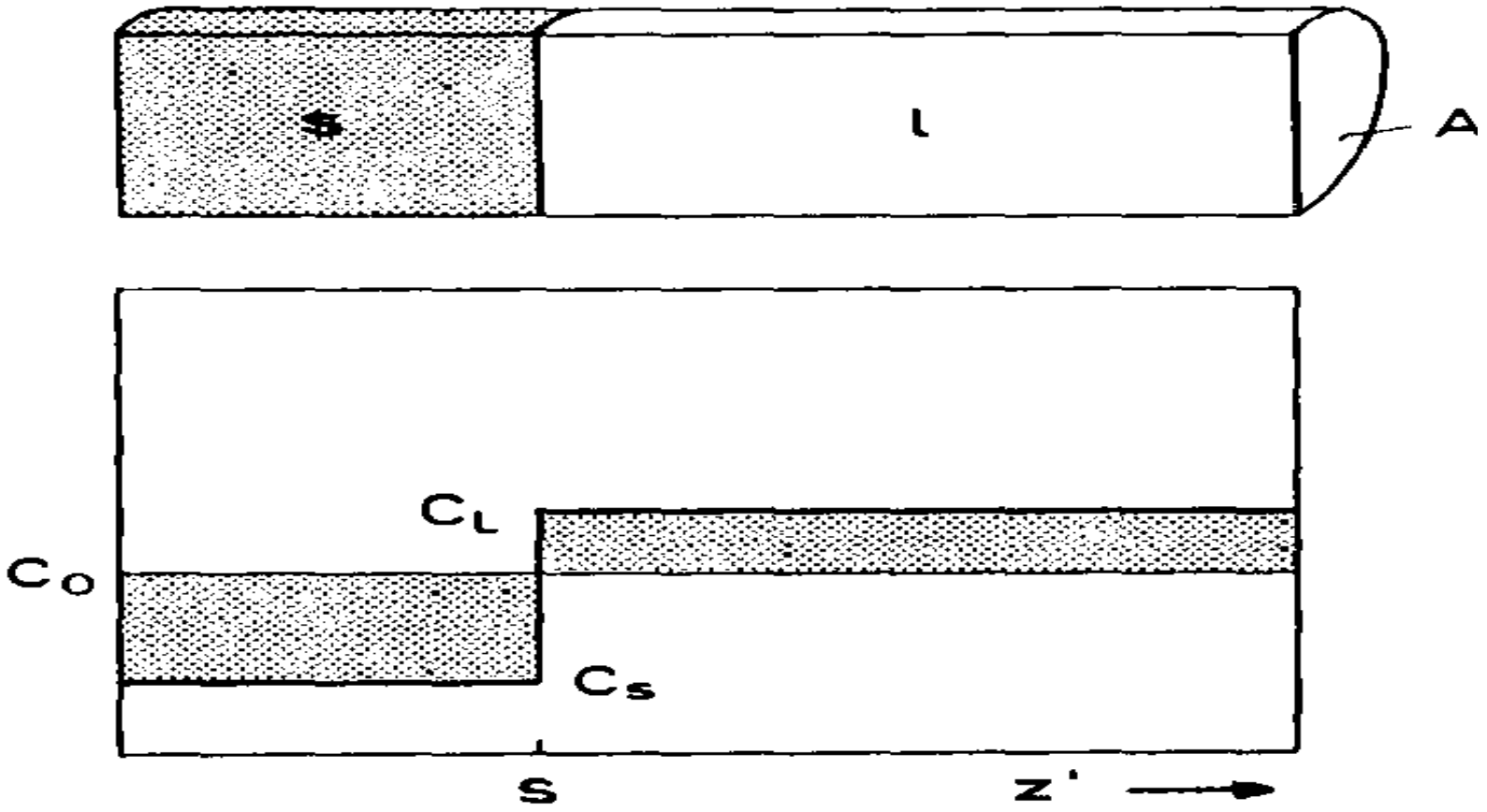

Lever Rule

The simplest case to which a mass balance can be applied is the case of equilibrium solidification (no concentration gradient in the solid or liquid). This can be expressed by the relations:

$$D_l \gg D_S \gg LV \qquad [A11.2]$$

Since L is the length of the solidifying system (figure A11.1), equation A11.2 states that the diffusion boundary layer, $\delta_c = 2D/V$, is much larger than the maximum distance, L, over which either solid or liquid state diffusion can occur. Similarly, it can be supposed that, if the growth rate, V, of the solid is constant and equal to L/t_f, the length of the specimen must be less than the characteristic diffusion length:

$$L \ll \sqrt{D_S t_f} \qquad [A11.3]$$

Under these conditions:

$$\frac{\partial C_l}{\partial z'} = \frac{\partial C_s}{\partial z'} \simeq 0$$

Taking the differential form of equation A11.1, $C_S = kC_l$, $dC_S = kdC_l$, $f_S = 1-f_l$, and $df_S = -df_l$ can be substituted and integrations performed:

$$\int_{C_o}^{C_l} \frac{dC_l}{pC_l} = \int_{o}^{f_s} \frac{df_S}{1 - f_S p}$$

$$\frac{C_l}{C_o} = \frac{1}{1 - pf_S}$$

$$p=1-k$$

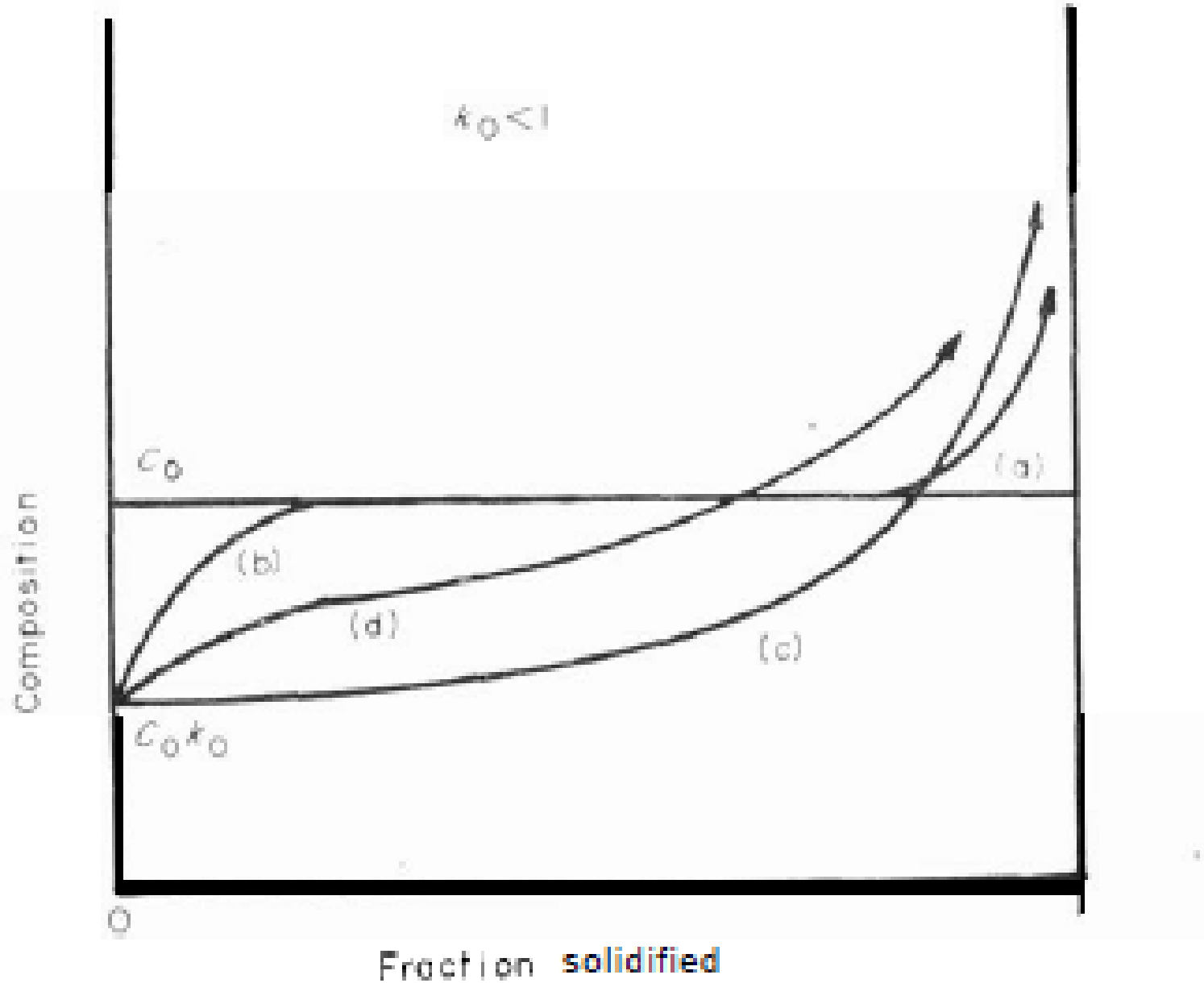

Fig. 4.13 Solute distributions in a solid bar frozen from liquid of initial concentration C_0, for: (a) equilibrium freezing; (b) solute mixing in the liquid by diffusion only; (c) complete solute mixing in the liquid; (d) partial solute mixing in the liquid.

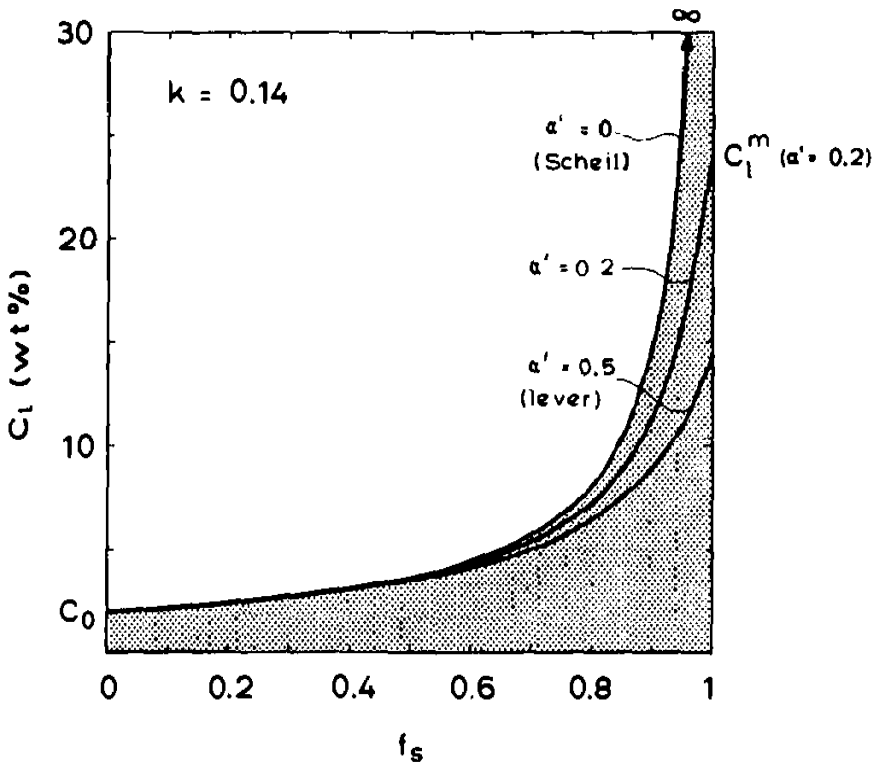

Figure 6.4: SEGREGATION CURVES IN THE PRESENCE OF BACK DIFFUSION. The composition of the liquid (assumed to be homogeneous as in figure 6.3) increases at the end of the specimen. Under lever-rule conditions, the increase is from C_0 to C_0/k, while the Scheil equation predicts an increase from C_0 to infinity. All of the intermediate cases can be described by one relationship (equation 6.9) which contains a modified α-parameter, α', which can take values between 0 and 0.5. Note that the curve represents the path of the interface concentration, C_l^*, as a function of f_s. The final solute distribution profile in the solid cannot be determined in this way because it changes with time when $\alpha > 0$. Therefore, only the end concentration ($f_s = 1$) represents a measurable value.

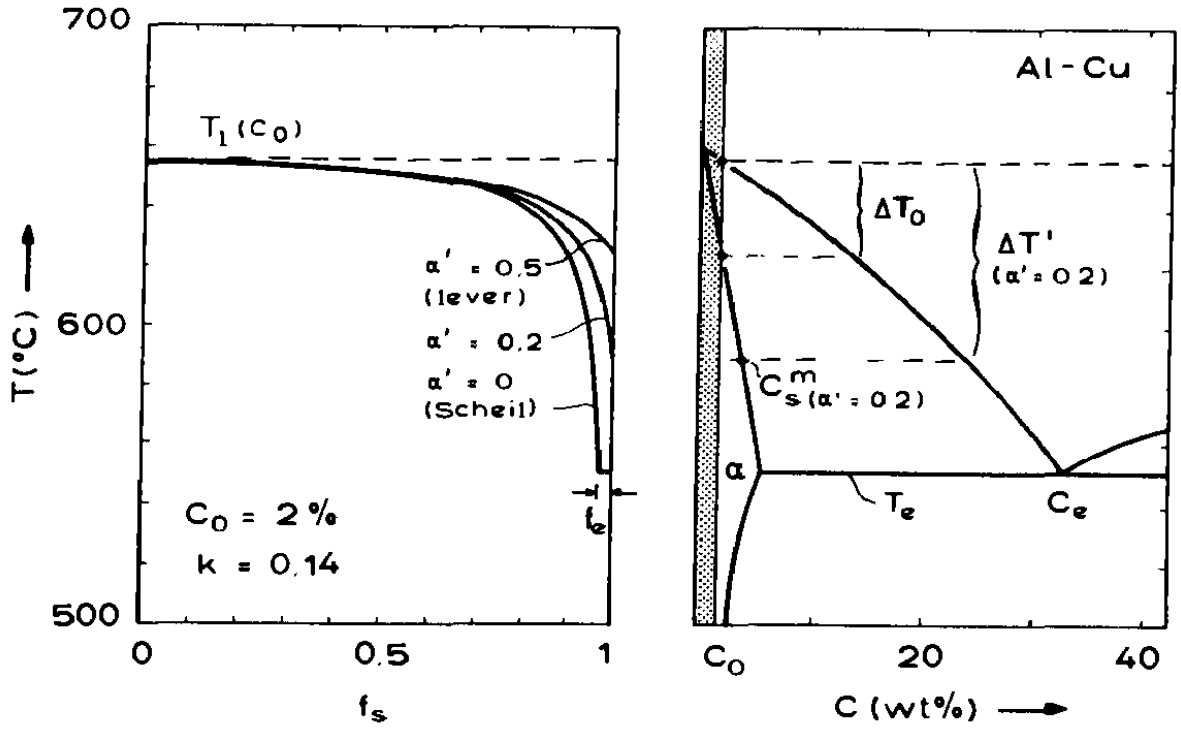

Figure 6.5: RELATIONSHIP OF THE SEGREGATE FREEZING POINT TO THE PHASE DIAGRAM. An increasing concentration (for distribution coefficients less than unity) is associated with a decreasing liquidus temperature since the slope, m, is then less than zero. Using the curves of figure 6.4, the temperature of the liquid as a function of volume fraction solidified can be derived. The use of realistic diffusion coefficients shows that, for small systems (such as interdendritic regions - figure 6.6) interstitial C in delta- and gamma-Fe will behave according to the lever-rule. Hence, the last liquid of a binary Fe-C melt will solidify at a temperature close to the solidus while substitutional alloys, such as Al-Cu, which typically have much smaller solid-state diffusion coefficients will usually contain eutectic material in the last (interdendritic) regions to solidify even when the overall composition is less than the solubility limit at T_e.

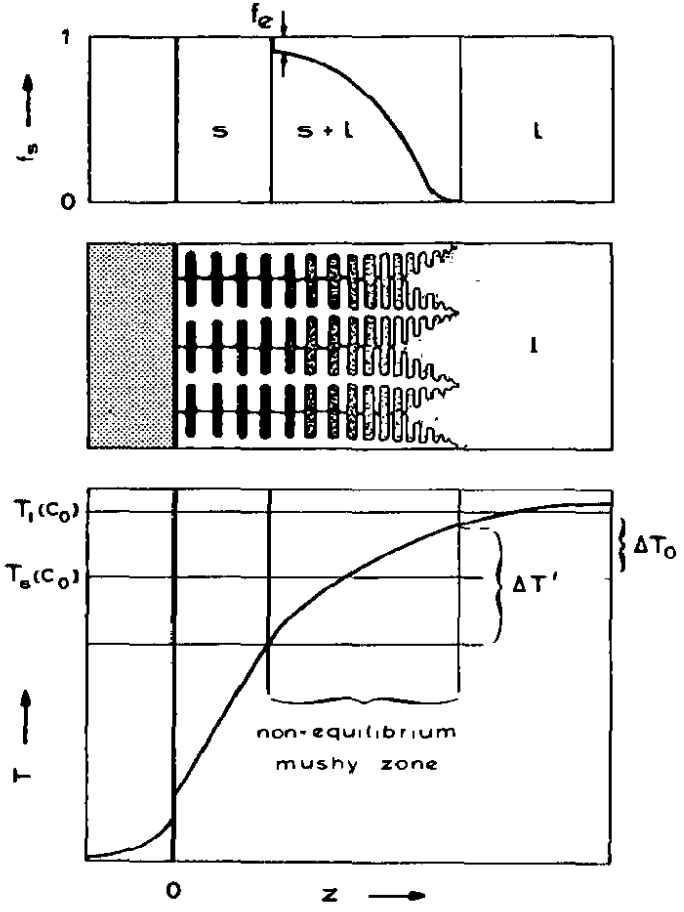

Figure 6.7: MICROSEGREGATION. The equilibrium melting range, ΔT_o does not, except for the lever rule case, correspond to the range, $\Delta T'$, over which the mushy zone develops. The dendrite tips need a certain undercooling which is determined by the stability of the tip. The dendrite roots will usually have much higher concentrations than C_o/k, due to non-equilibrium solidification. This often leads to interdendritic precipitation of eutectic phases of volume fraction, f_e, even if the composition is not on the eutectic tie-line. In the columnar zone of a casting, as shown here, the volume fraction of solid, f_s, will follow an S-shaped curve like that in the uppermost diagram.

- **1 no mixing in liquid no diffusion in solid no coarsening**
- 2. partial mixing in liquid no diffusion in solid no coarsening
- 3. complete mixing in liquid no diffusion in solid no coarsening
- 4. complete mixing in liquid diffusion in solid no coarsening
- 5. complete mixing in liquid diffusion in solid coarsening
- 6. complete mixing in liquid complete diffusion in solid

1 model

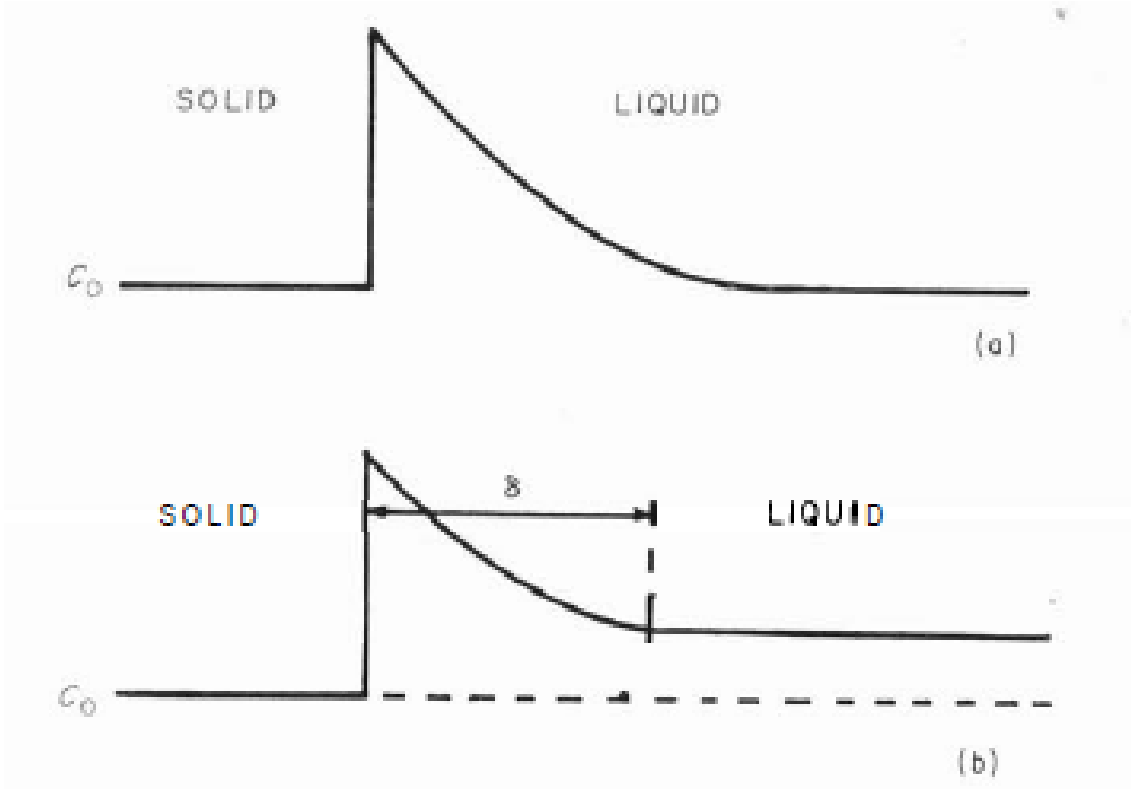

Fig. 4.12. The effect of the mixing conditions on the nature of the solute layer at the interface: (a) no mixing, diffusion only; (b) partial mixing; (c) complete mixing.

$$D\frac{\mathrm{d}^2C}{\mathrm{d}x^2} + R\frac{\mathrm{d}C}{\mathrm{d}x} = 0$$

$$C = C_0\left[1 + \frac{1 - k_0}{k_0}\exp\left(-\frac{Rx}{D}\right)\right]$$

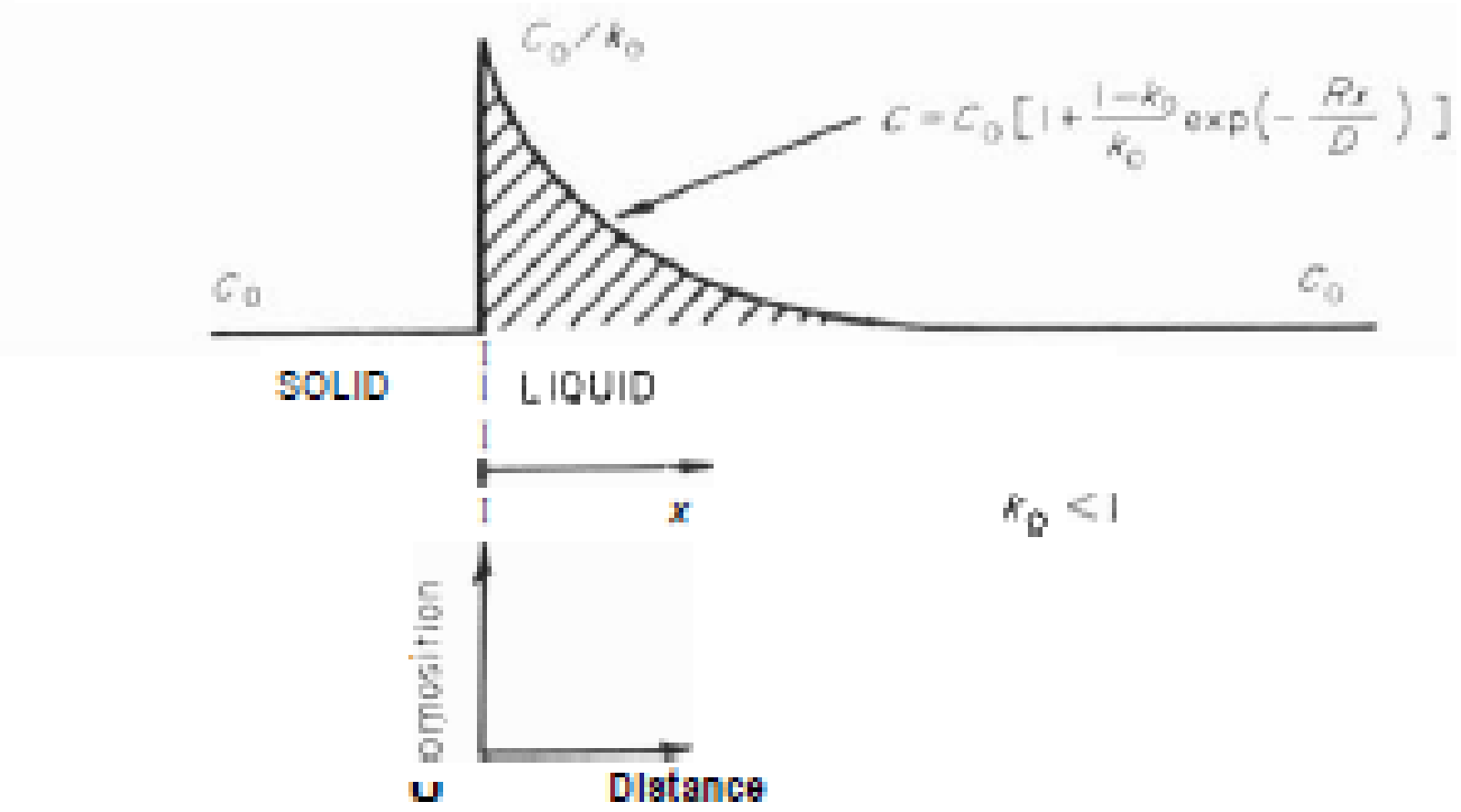

Fig. 4.7 *The solute profile ahead of the interface during steady-state solidification with solute redistribution by diffusion only* ($k_0 < 1$).

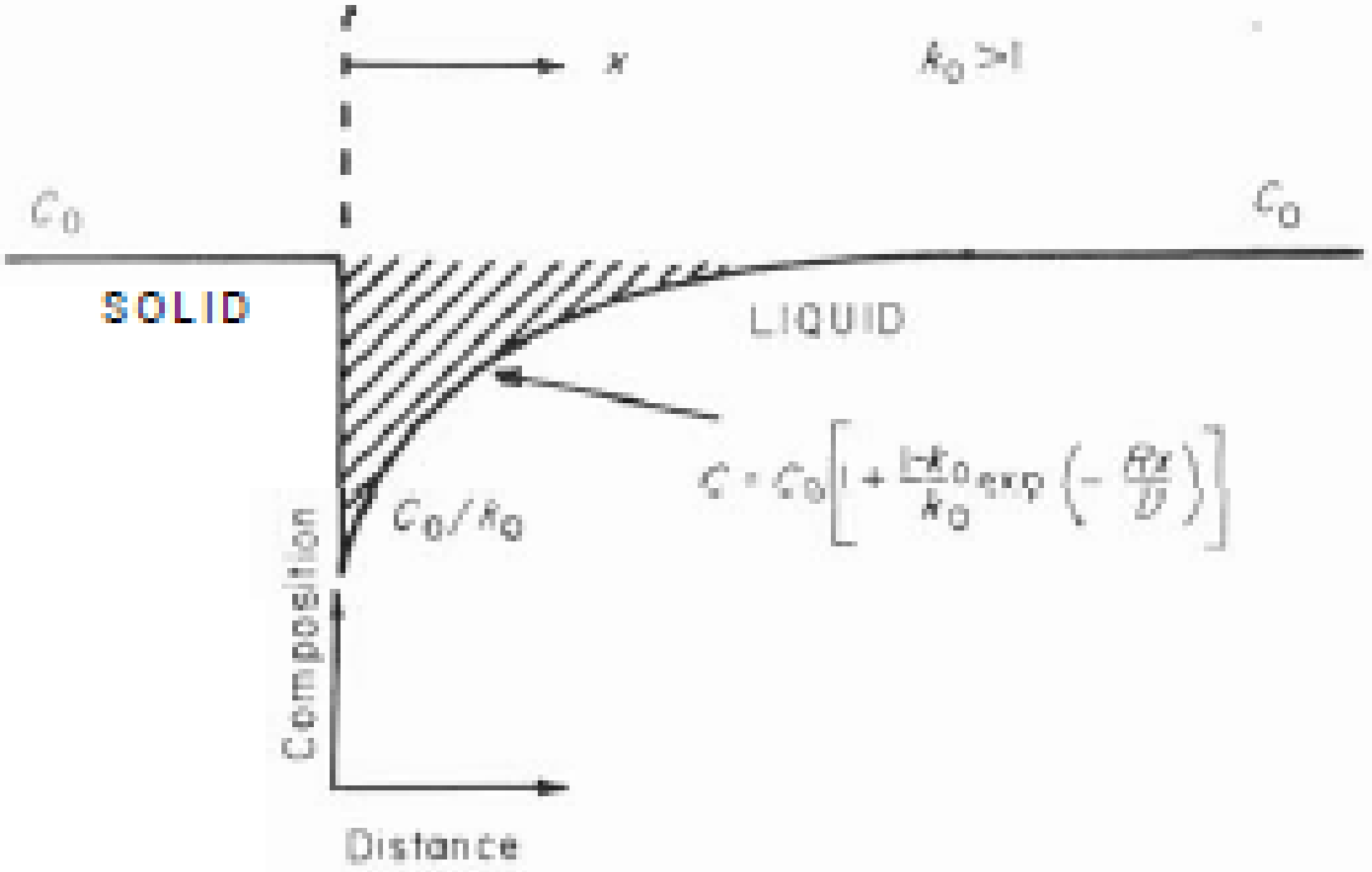

Fig. 4.8 The corresponding profile to that of Fig. 4.7 for $k_0 > 1$.

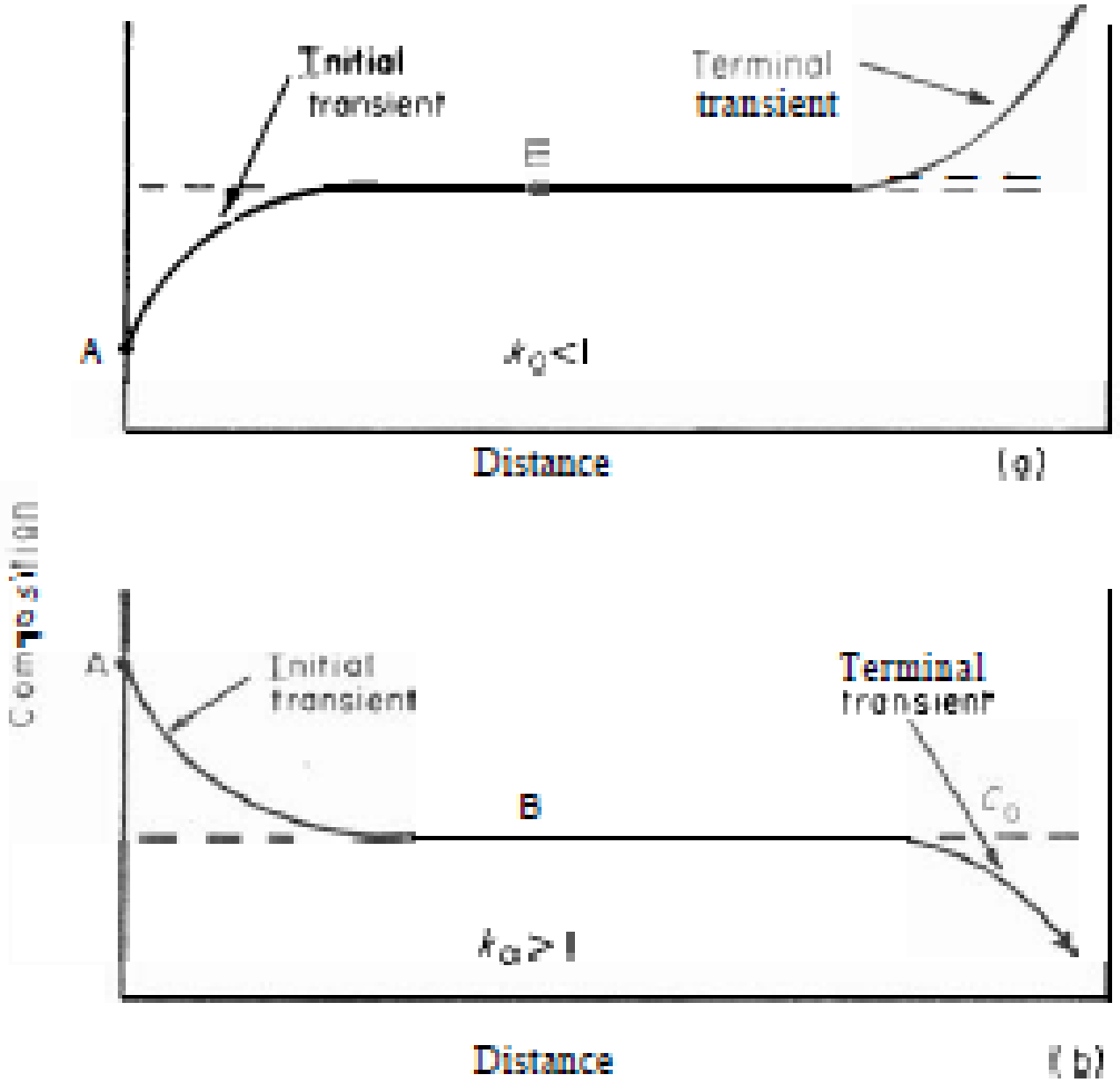

Fig. 4.10 Concentration–distance profiles for a bar solidified under condition where solute transport in the liquid is by diffusion only: (a) $k_0 < 1$; *(b)* $k_0 > 1$.

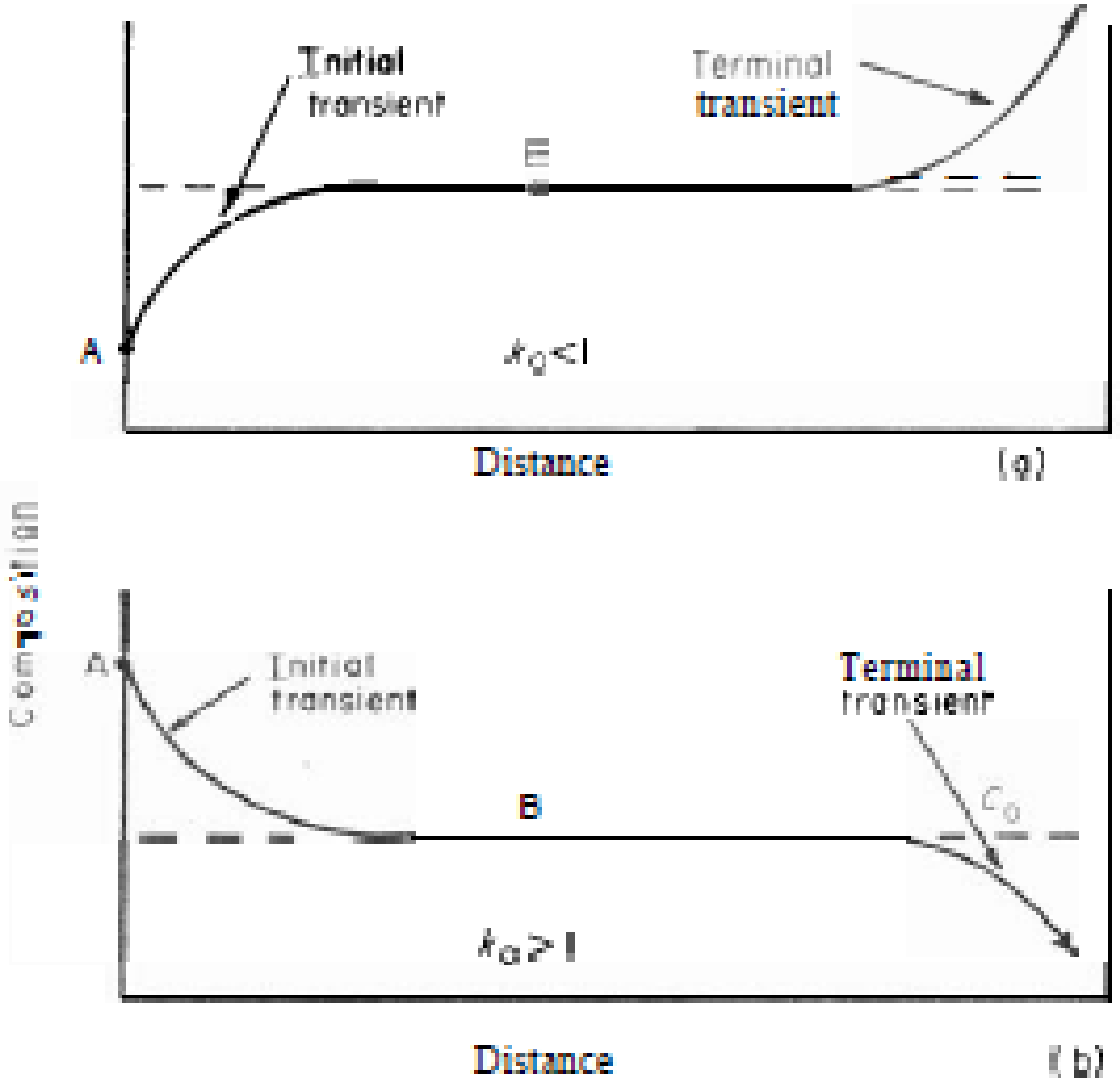

Fig. 4.10 Concentration–distance profiles for a bar solidified under condition where solute transport in the liquid is by diffusion only: (a) $k_0 < 1$; *(b)* $k_0 > 1$.

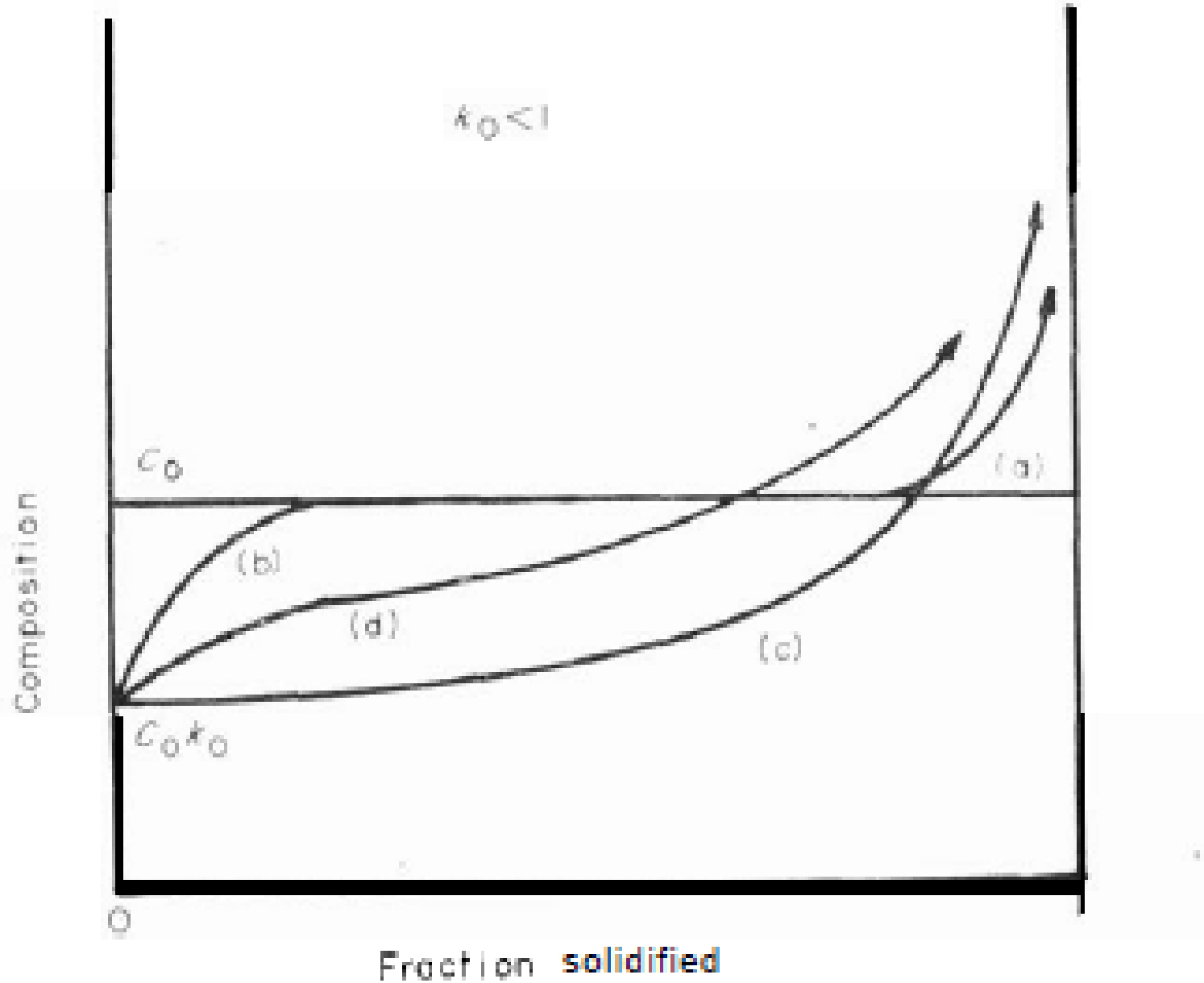

Fig. 4.13 Solute distributions in a solid bar frozen from liquid of initial concentration C_0, for: (a) equilibrium freezing; (b) solute mixing in the liquid by diffusion only; (c) complete solute mixing in the liquid; (d) partial solute mixing in the liquid.

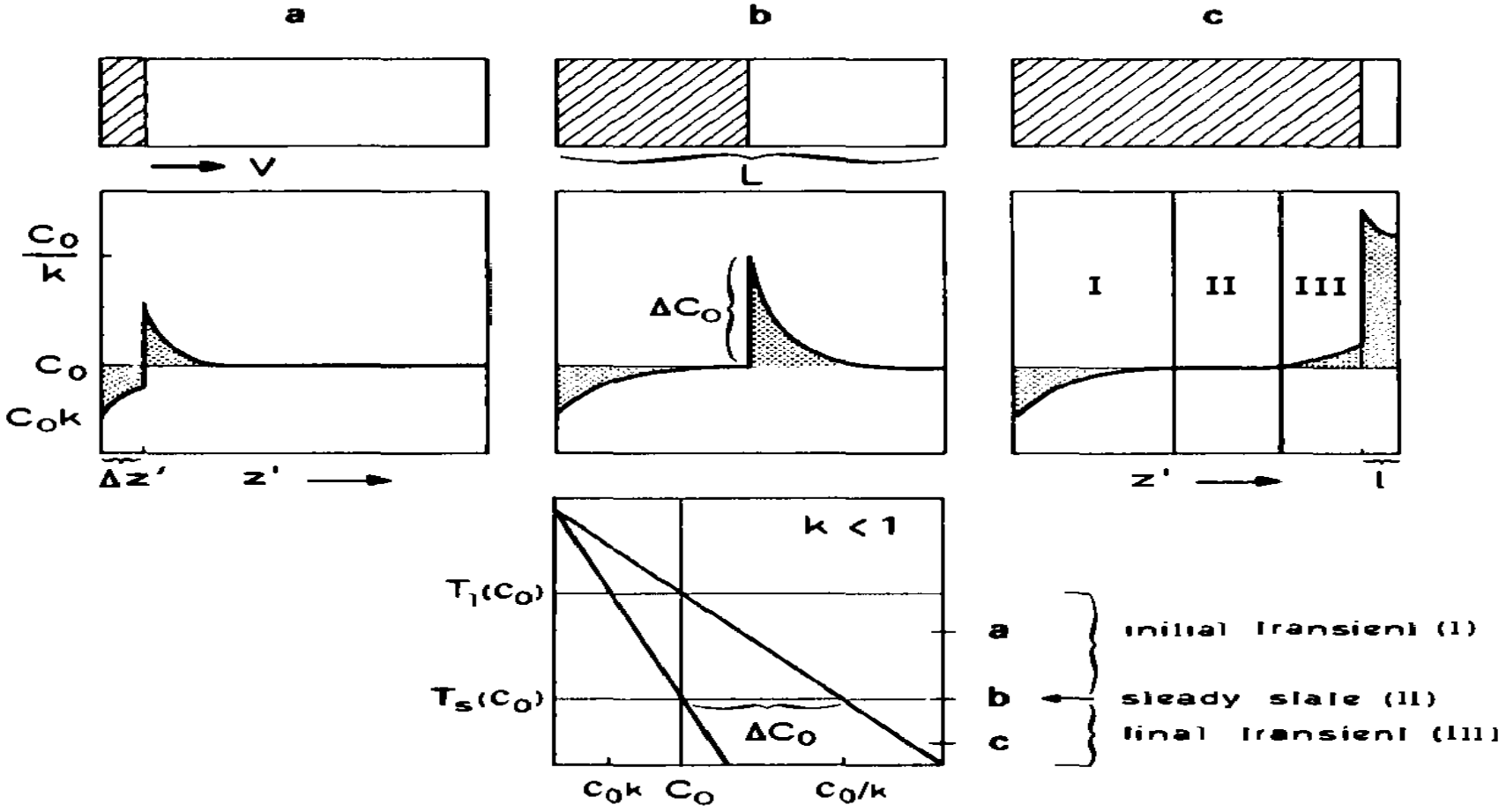
a
b
c
V
L
$\frac{C_0}{k}$
C_0
C_{0k}
ΔC_0
I
II
III
$\Delta z'$
z'
l
k < 1
$T_l(C_0)$
$T_s(C_0)$
ΔC_0
C_{0k}
C_0
C_0/k
a
b
c
initial transient (I)
steady state (II)
final transient (III)

- 1 no mixing in liquid no diffusion in solid no coarsening
- **2. partial mixing in liquid no diffusion in solid no coarsening**
- 3. complete mixing in liquid no diffusion in solid no coarsening
- 4. complete mixing in liquid diffusion in solid no coarsening
- 5. complete mixing in liquid diffusion in solid coarsening
- 6. complete mixing in liquid complete diffusion in solid

2 model

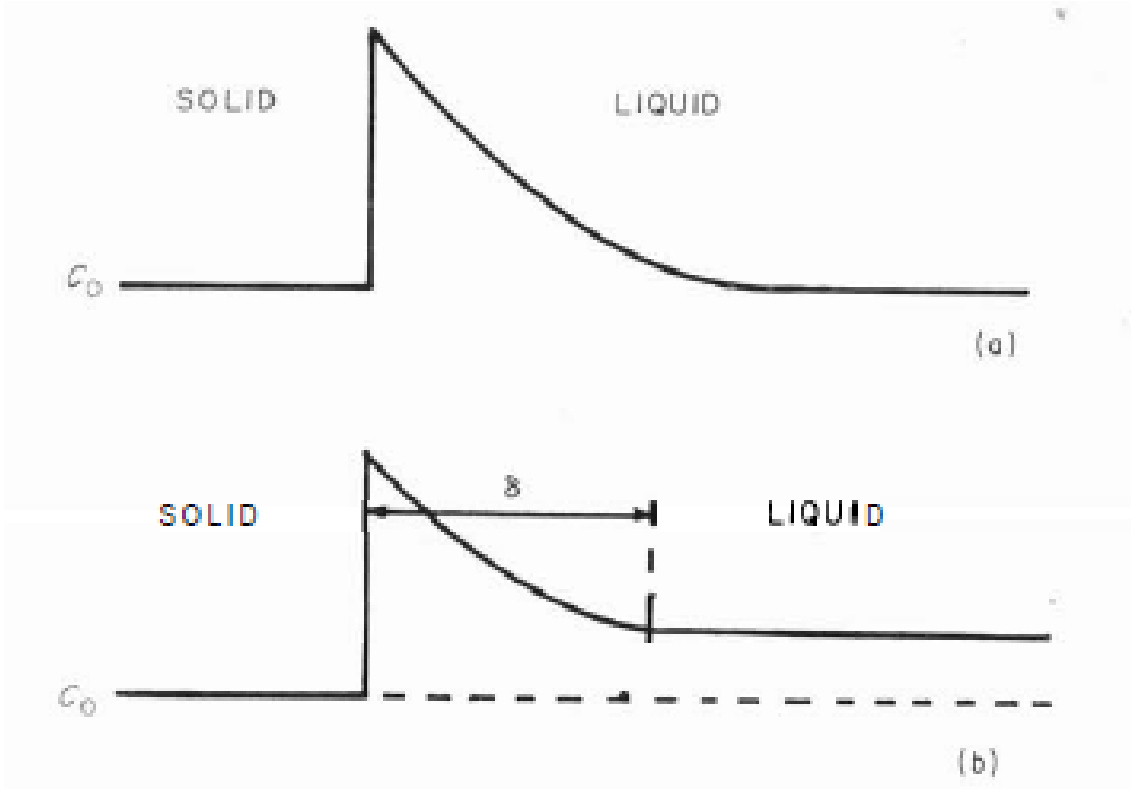

Fig. 4.12 The effect of the mixing conditions on the nature of the solute layer at the interface: (a) no mixing, diffusion only; (b) partial mixing; (c) complete mixing.

the *effective* distribution coefficient is given by

$$k_E = \frac{k_0}{k_0 + (1 - k_0)\exp[-(R\delta/D)]}$$

$$C_s = C_0 k_E (1 - x)^{k_0 - 1}$$

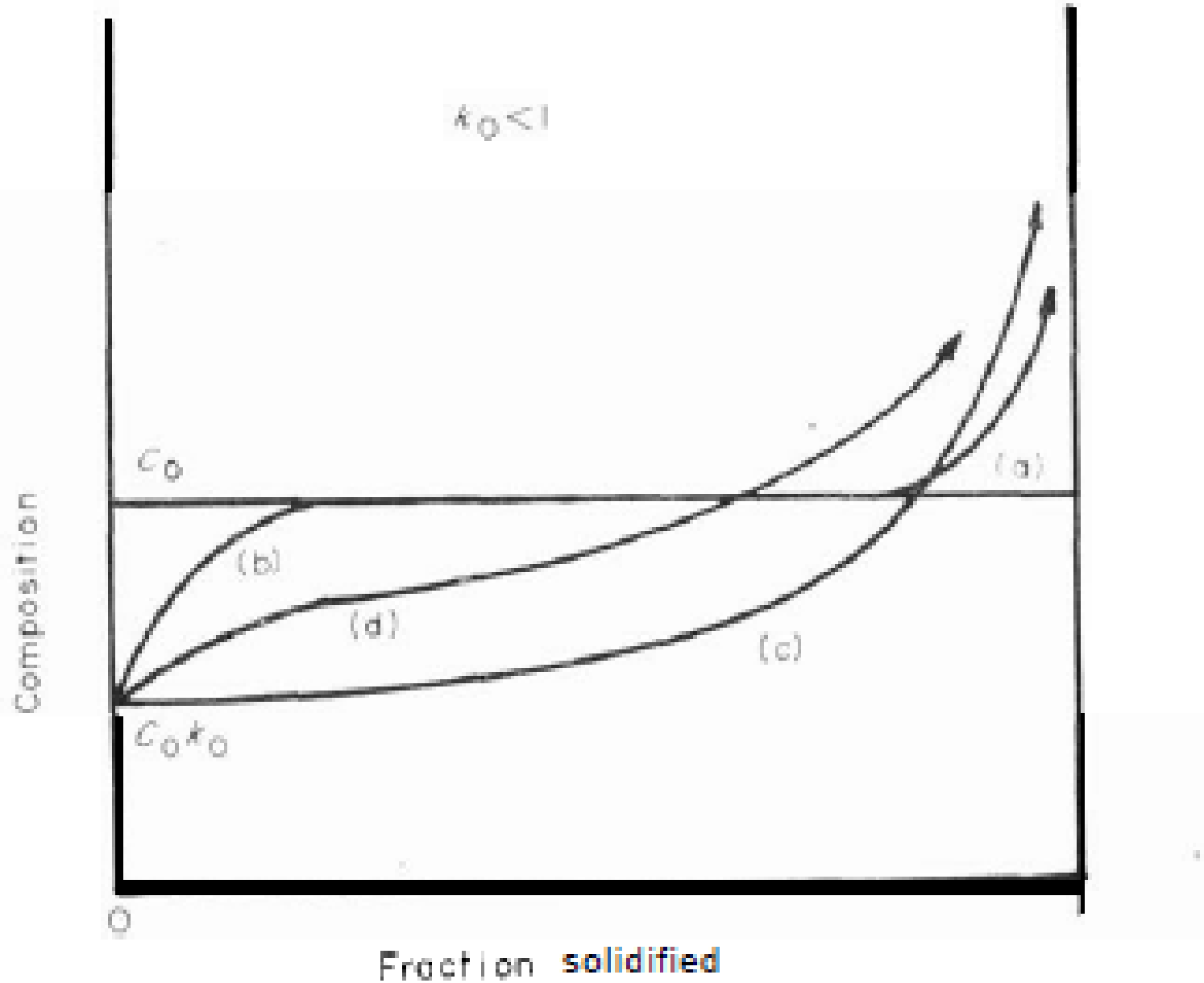

Fig. 4.13 Solute distributions in a solid bar frozen from liquid of initial concentration C_0, for: (a) equilibrium freezing; (b) solute mixing in the liquid by diffusion only; (c) complete solute mixing in the liquid; (d) partial solute mixing in the liquid.

- 1 no mixing in liquid no diffusion in solid no coarsening
- 2. partial mixing in liquid no diffusion in solid no coarsening
- **3. complete mixing in liquid no diffusion in solid no coarsening**
- 4. complete mixing in liquid diffusion in solid no coarsening
- 5. complete mixing in liquid diffusion in solid coarsening
- 6. complete mixing in liquid complete diffusion in solid

Introduction

Microsegregation is a distribution of solute elements in dendritic or cellular cast structures and can affect mechanical and chemical properties and phase transformations in alloys, such as homogenization and solution heat treatments, pearlite-ferrite banding structure, martensitic transformation and corrosion.

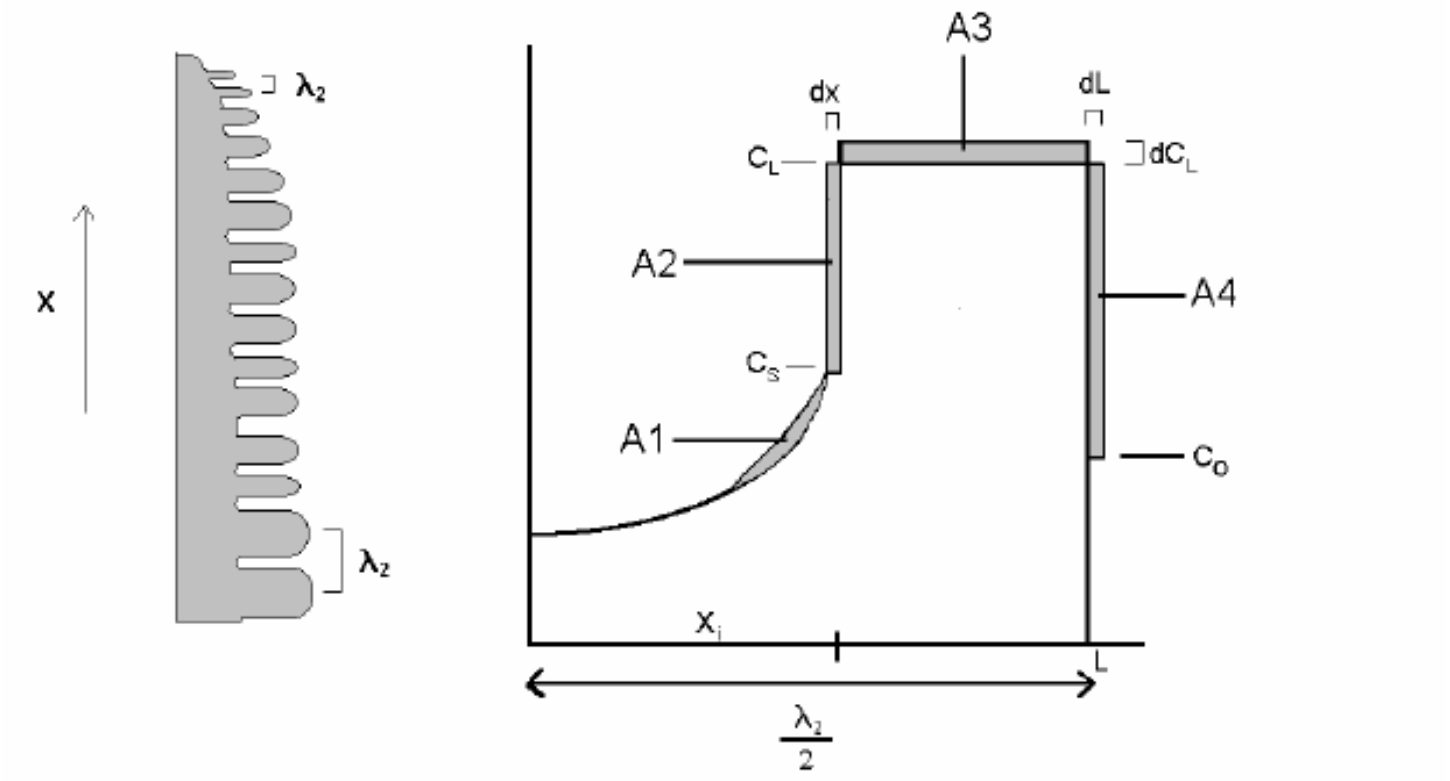

Figure 1 Dimensional form of microsegregation volume element from the centre of side arm to the centre of the liquid pool

In literature, many attempts have been done in order to analyze solute distribution during solidification of a binary or a multicomponent alloy. The first and simplest analytical model for a binary alloy came from Gulliver-Scheil, considering a constant partition coefficient at the interface during solidification [1,2]. In addition to this, they assumed that there is:

1. No difference in the density between solid and liquid
2. Constant physical properties
3. Complete mixing in the liquid
4. No effect of macrosegregation
5. Plate-like morphology at the solid -liquid interface
6. No back diffusion in the solid during solidification
7. Constant volume element, i.e. no dendrite arm coarsening,
8. No undercooling at the tip of dendrite at the beginning of solidification
9. No effect of temperature gradient zone melting (TGZM) on solute distribution.

The partial differential equation of Gulliver-Scheil model for these conditions can be written due to fig.1 as follows:

$A_2=A_3$

$$(C_L - C_S)\frac{dx_i}{dt} = (L - X_i)\frac{dC_L}{dt}. \qquad (1)$$

The analytical solution of this differential equation is:

$$C_S = kC_O\left(1 - f_S\right)^{(k-1)}.$$

CL=Co(1-fs)^(k-1)

CL=Cofl^(k-1)

Cs=kCofl^(k-1)

fs+fl=1 k=Cs/Cl

$$f_s = \frac{1}{1 - 2\alpha' k} \left[1 - \frac{T_f - T}{T_f - T_i} \right]^{\frac{1 - 2\alpha' k}{k - 1}}$$

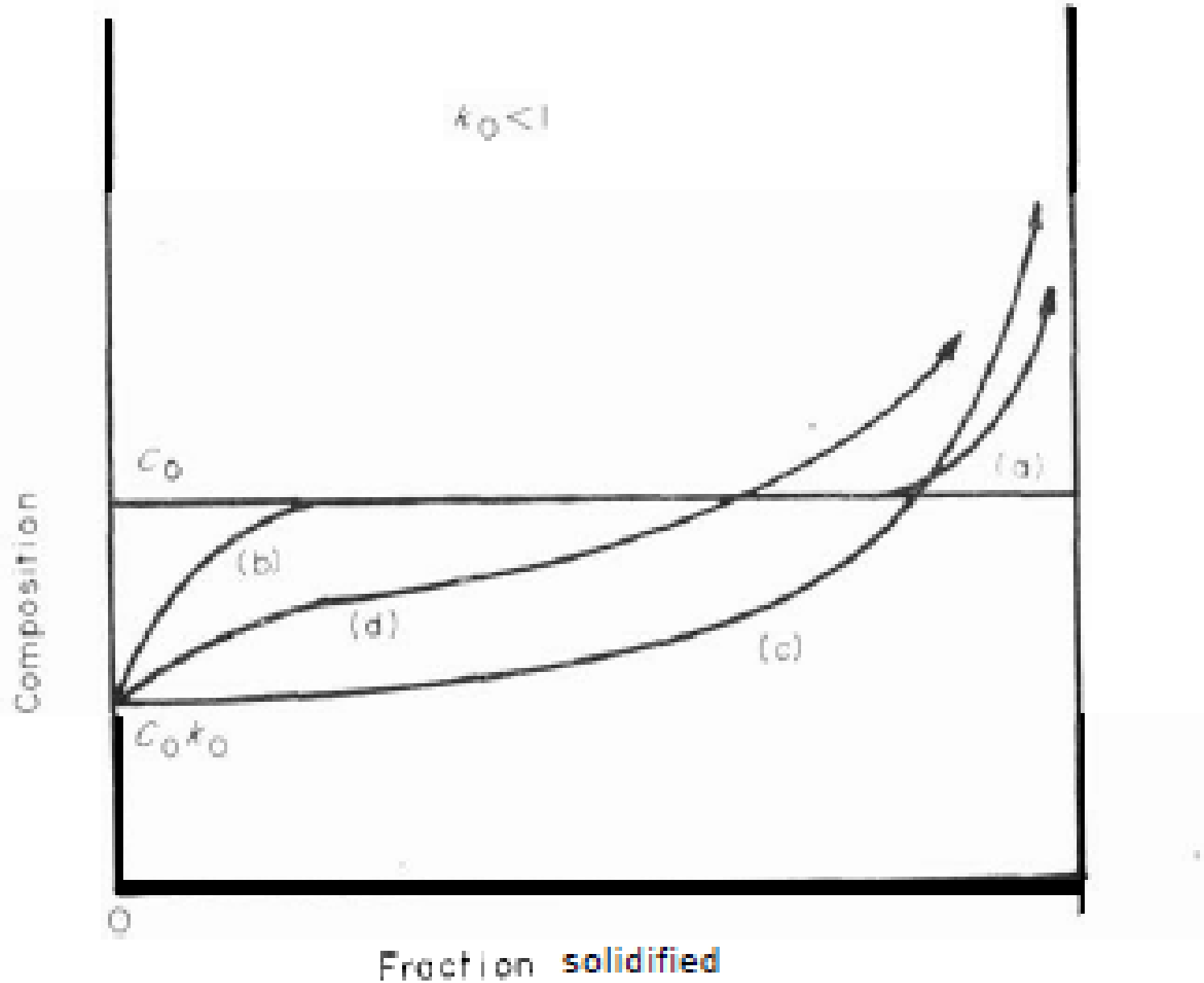

Fig. 4.13 Solute distributions in a solid bar frozen from liquid of initial concentration C_0, for: (a) equilibrium freezing; (b) solute mixing in the liquid by diffusion only; (c) complete solute mixing in the liquid; (d) partial solute mixing in the liquid.

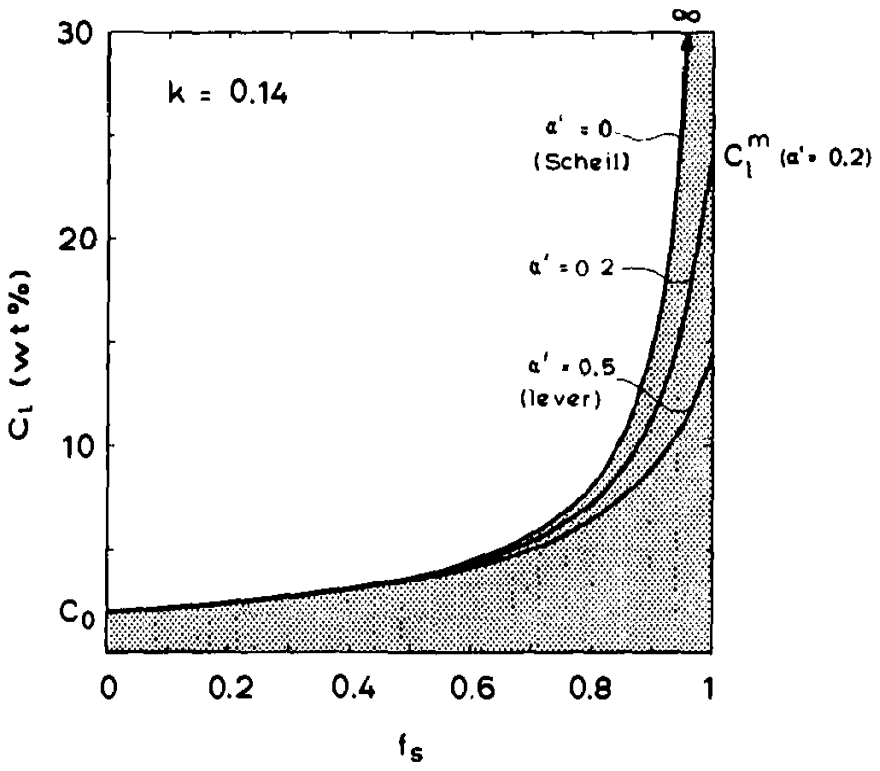

Figure 6.4: SEGREGATION CURVES IN THE PRESENCE OF BACK DIFFUSION. The composition of the liquid (assumed to be homogeneous as in figure 6.3) increases at the end of the specimen. Under lever-rule conditions, the increase is from C_0 to C_0/k, while the Scheil equation predicts an increase from C_0 to infinity. All of the intermediate cases can be described by one relationship (equation 6.9) which contains a modified α-parameter, α', which can take values between 0 and 0.5. Note that the curve represents the path of the interface concentration, C_l^*, as a function of f_s. The final solute distribution profile in the solid cannot be determined in this way because it changes with time when $\alpha > 0$. Therefore, only the end concentration ($f_s = 1$) represents a measurable value.

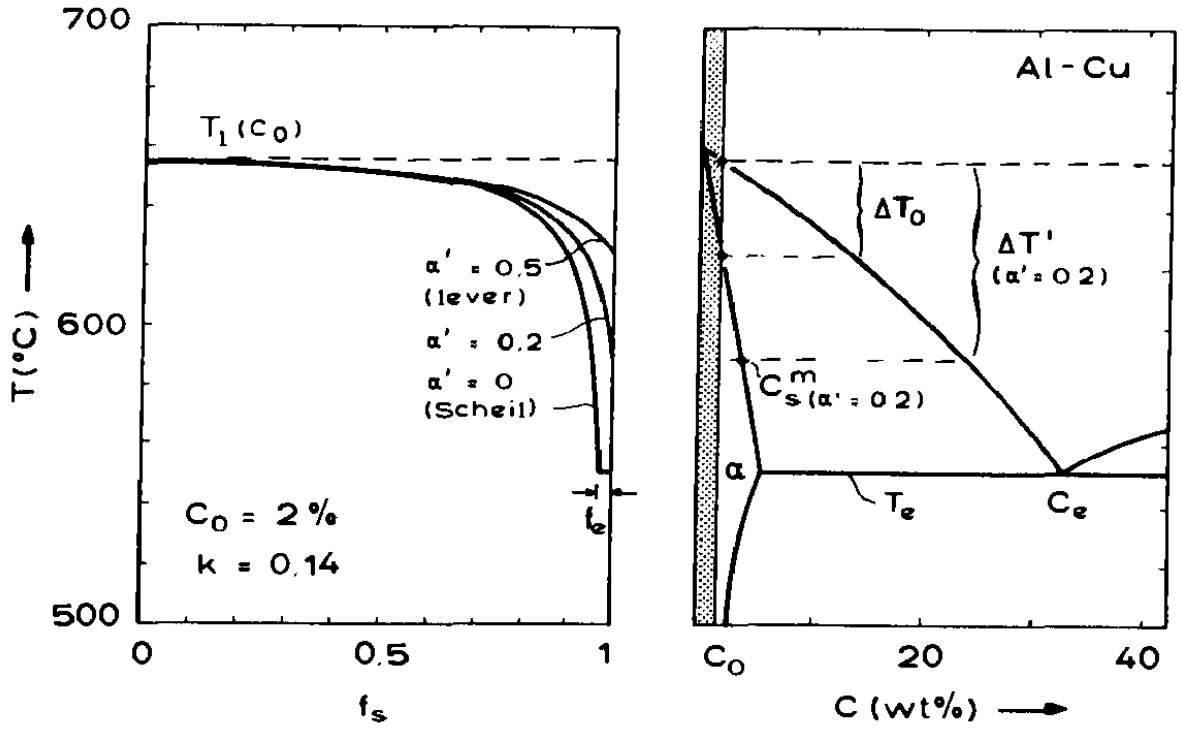

Figure 6.5: RELATIONSHIP OF THE SEGREGATE FREEZING POINT TO THE PHASE DIAGRAM. An increasing concentration (for distribution coefficients less than unity) is associated with a decreasing liquidus temperature since the slope, m, is then less than zero. Using the curves of figure 6.4, the temperature of the liquid as a function of volume fraction solidified can be derived. The use of realistic diffusion coefficients shows that, for small systems (such as interdendritic regions - figure 6.6) interstitial C in delta- and gamma-Fe will behave according to the lever-rule. Hence, the last liquid of a binary Fe-C melt will solidify at a temperature close to the solidus while substitutional alloys, such as Al-Cu, which typically have much smaller solid-state diffusion coefficients will usually contain eutectic material in the last (interdendritic) regions to solidify even when the overall composition is less than the solubility limit at T_e.

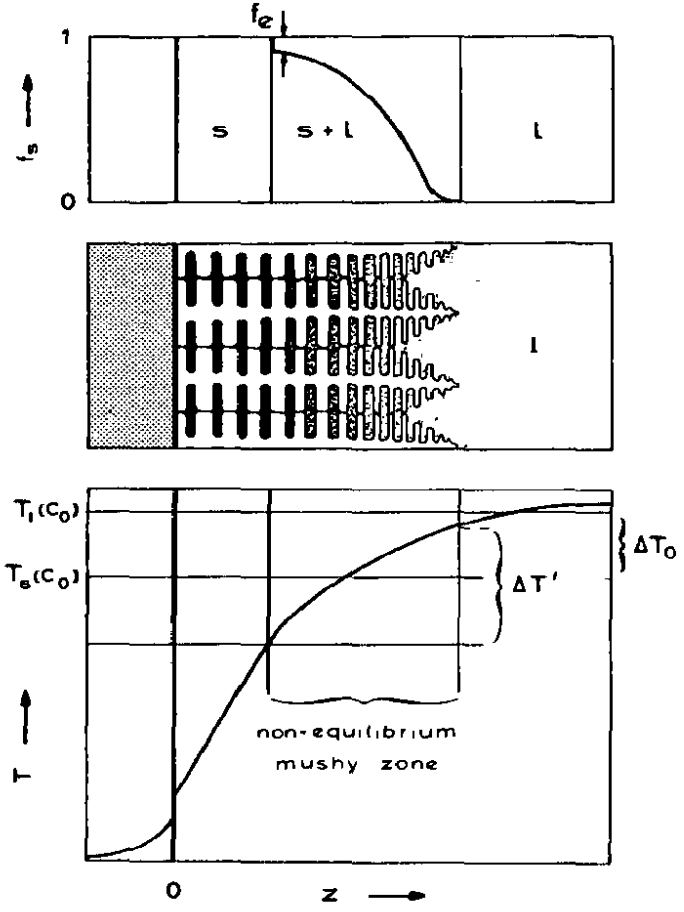

Figure 6.7: MICROSEGREGATION. The equilibrium melting range, ΔT_o does not, except for the lever rule case, correspond to the range, $\Delta T'$, over which the mushy zone develops. The dendrite tips need a certain undercooling which is determined by the stability of the tip. The dendrite roots will usually have much higher concentrations than C_o/k, due to non-equilibrium solidification. This often leads to interdendritic precipitation of eutectic phases of volume fraction, f_e, even if the composition is not on the eutectic tie-line. In the columnar zone of a casting, as shown here, the volume fraction of solid, f_s, will follow an S-shaped curve like that in the uppermost diagram.

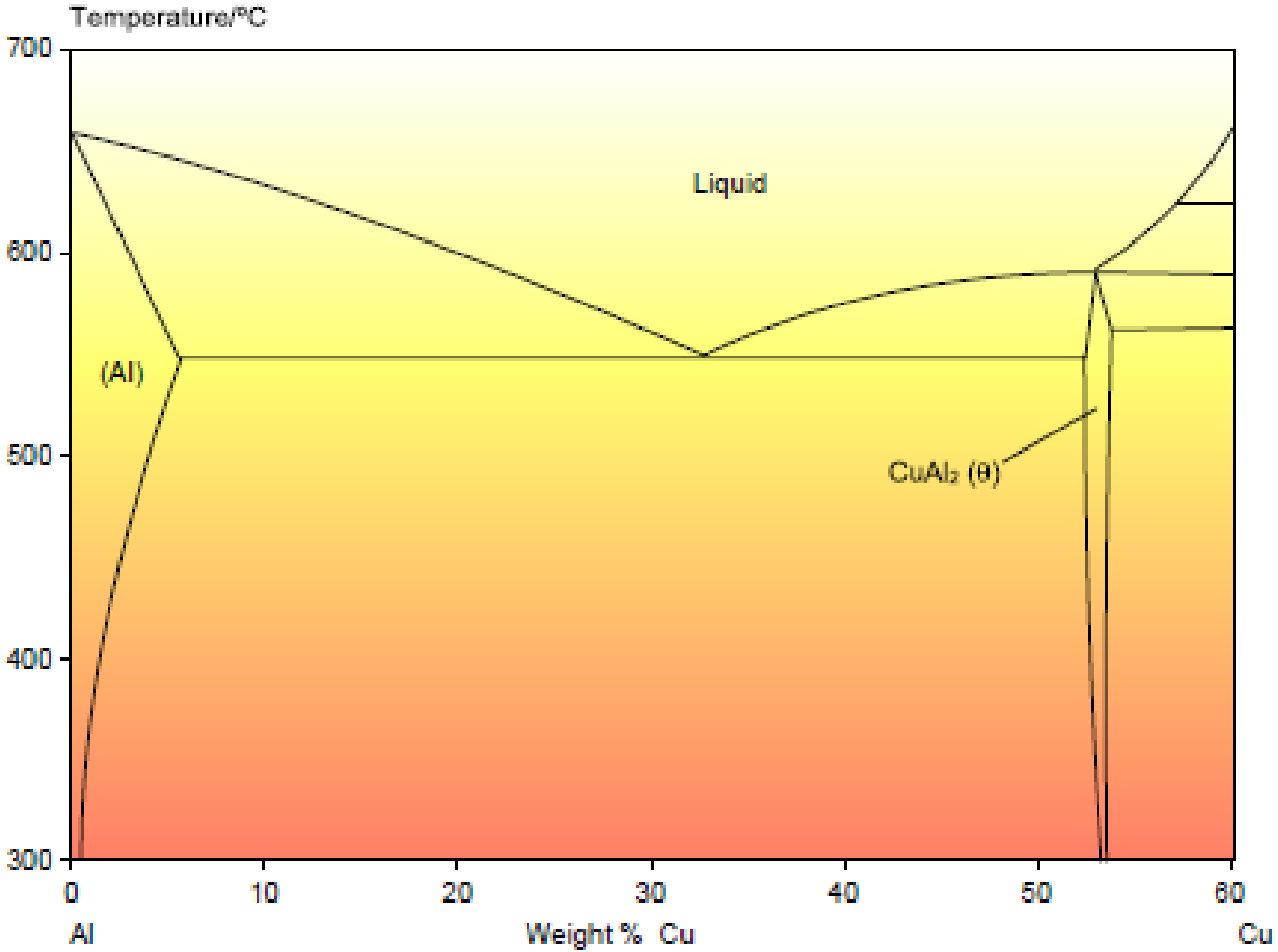
Temperature/°C
700
600
500
400
300
Liquid
(Al)
CuAl2 (θ)
0
10
20
30
40
50
60
Al
Weight % Cu
Cu

Co=4.5

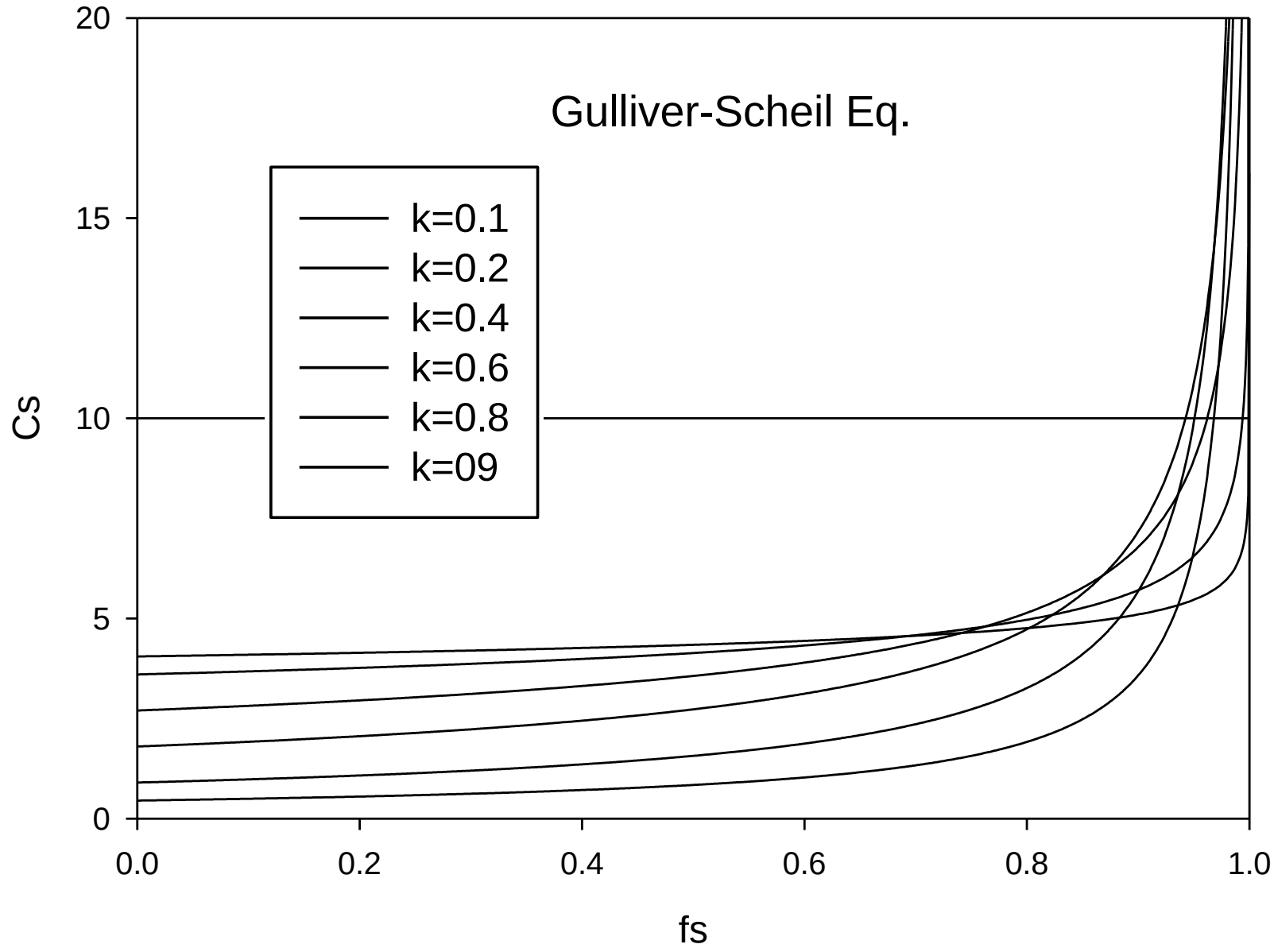
Gulliver-Scheil Eq.
k=0.1
k=0.2
k=0.4
k=0.6
k=0.8
k=09
Cs
fs
0
5
10
15
20
0.0
0.2
0.4
0.6
0.8
1.0

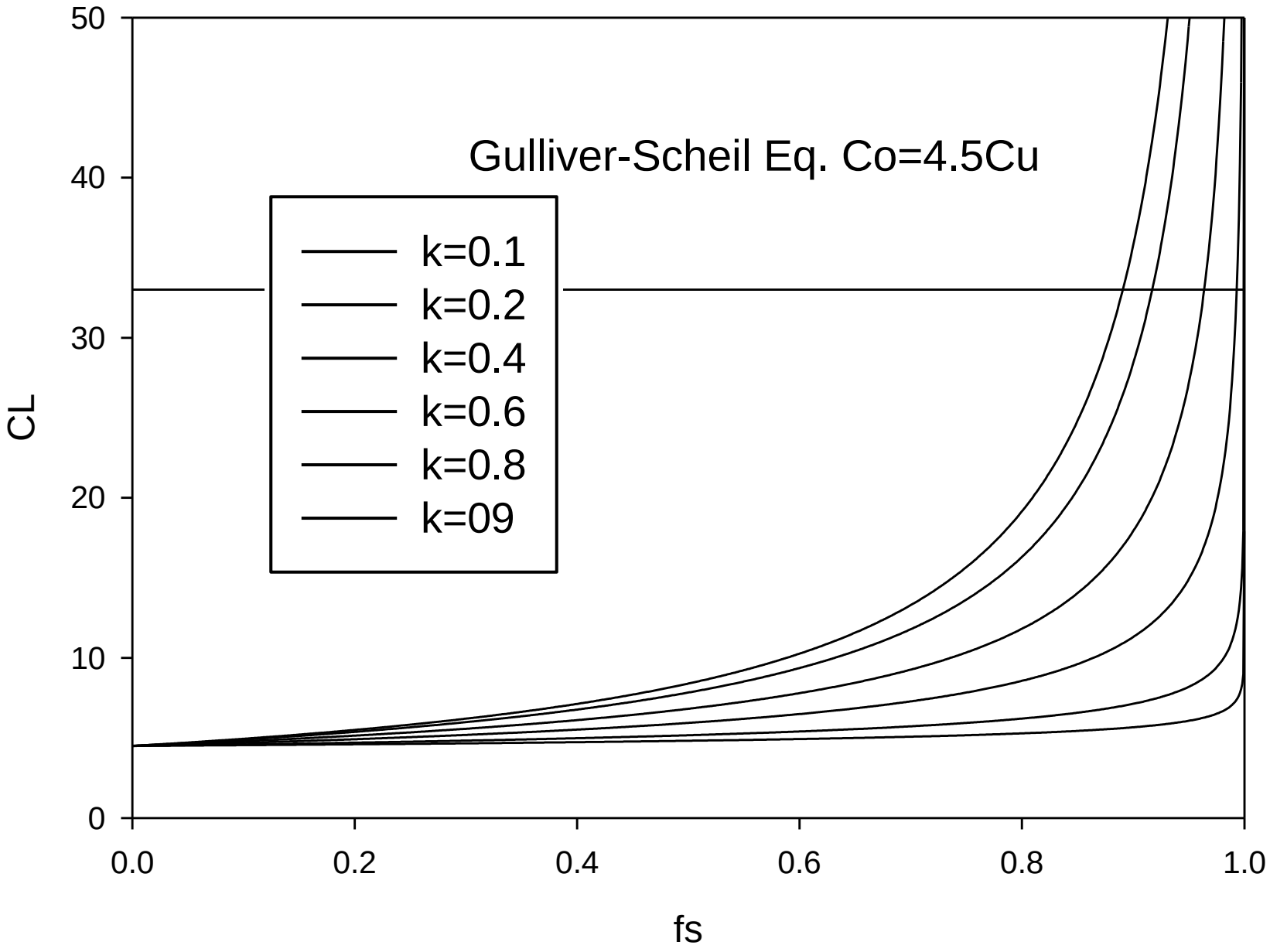
Gulliver-Scheil Eq. Co=4.5Cu
k=0.1
k=0.2
k=0.4
k=0.6
k=0.8
k=09
CL
fs
0
10
20
30
40
50
0.0
0.2
0.4
0.6
0.8
1.0

- 1 no mixing in liquid no diffusion in solid no coarsening
- 2. partial mixing in liquid no diffusion in solid no coarsening
- 3. complete mixing in liquid no diffusion in solid no coarsening
- **4. complete mixing in liquid diffusion in solid no coarsening**
- 5. complete mixing in liquid diffusion in solid coarsening
- 6. complete mixing in liquid complete diffusion in solid

Later, it was seen that the assumption of no solid-state back diffusion during solidification was not true. Especially, this becomes important near to the end of solidification due to the steep concentration profile and also important in the solidification of body centered cubic structures, such as δ-Fe in steels. Brody-Flemings proposed an approximate analytical model, taking into account one dimensional diffusion of solute in solid during solidification in plate-like dendrite arms [3]. The other assumptions of the Gulliver-Scheil model were kept the same. From fig.1, the partial differential equation of Brody-Flemings model can be written as follows:

$A_2=A_3+A_1$

$$(C_L - C_S)\frac{dx_i}{dt} = D_S\left(\frac{dC}{dx}\right)_{X_i} + (L - X_i)\frac{dC_L}{dt}. \qquad (3)$$

Introduction

Microsegregation is a distribution of solute elements in dendritic or cellular cast structures and can affect mechanical and chemical properties and phase transformations in alloys, such as homogenization and solution heat treatments, pearlite-ferrite banding structure, martensitic transformation and corrosion.

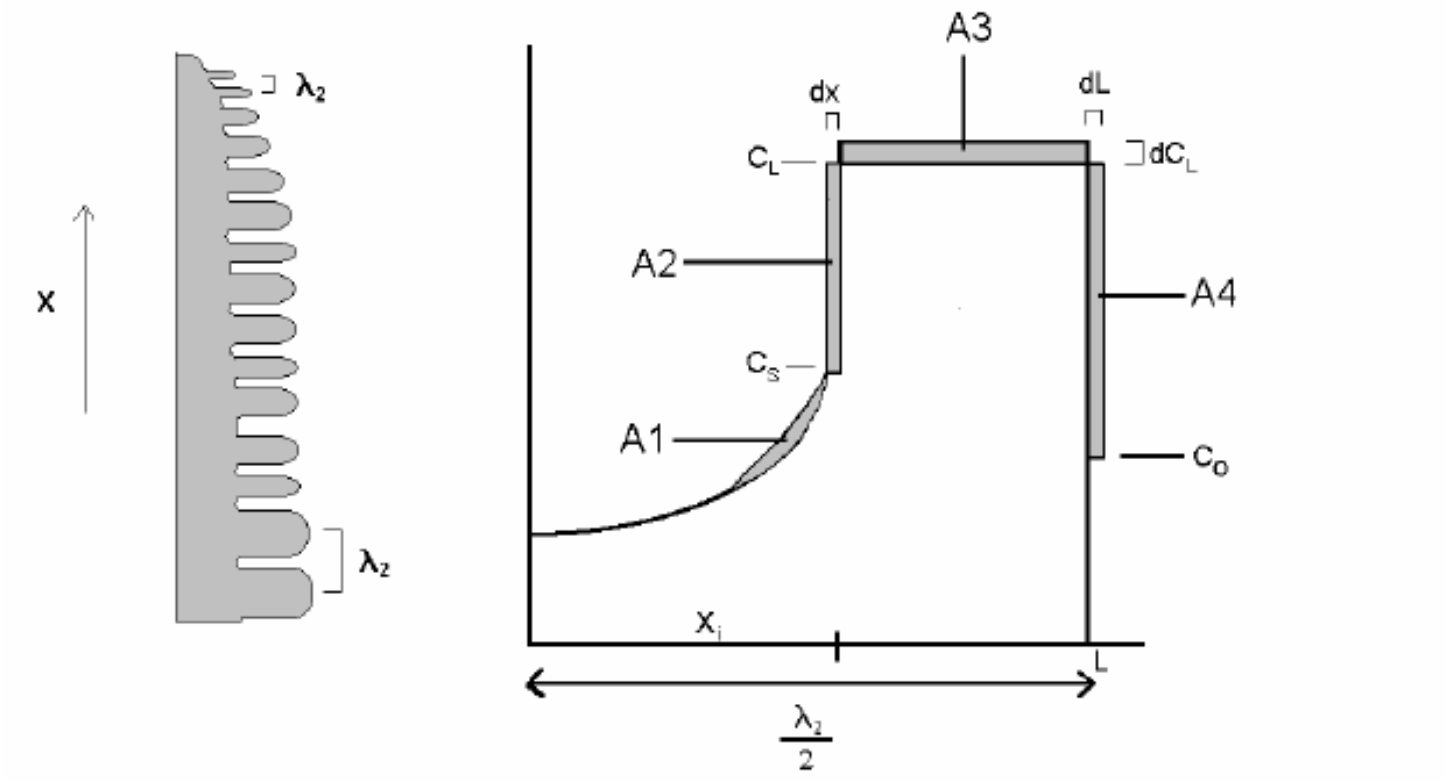

Figure 1 Dimensional form of microsegregation volume element from the centre of side arm to the centre of the liquid pool

The analytical solution of this differential equation for the parabolic growth rate is:

$$C_S = kC_O\left(1 - f_S(1 - 2k\alpha)\right)^{\left(\frac{k-1}{1-2\alpha k}\right)}.$$

Cs=kCo(1-(1-k*beta)*fs)^((k-1)/(1-k*beta))

The dimensionless parameter $\alpha=(D_S t_f)/L^2$ determines the extent of diffusion in the solid phase. Several authors criticized α dimensionless parameter for being not considered true back diffusion in solid, especially for rapid solid-state diffusion cases, $\alpha > 0.1$. For the parabolic growth rate, Clyne-Kurz replaced α parameter with Ω parameter which is also a function of α and but behave correctly over the whole range of α values for plate-like morphology [4].

$$\Omega(\alpha) = \alpha\left(1 - \exp\left(-\frac{1}{\alpha}\right)\right) - \frac{1}{2}\exp\left(-\frac{1}{2\alpha}\right). \quad (5)$$

Kirkwood modified the Brody-Flemings model for the dendrite arm coarsening situation [5]. He added the last term to the partial differential equation of Brody-Flemings This represents the

Beta=2*alpha/(1+2*alpha) Ohnaka

Beta=2*alpha/(1+2*alpha+1/2k)

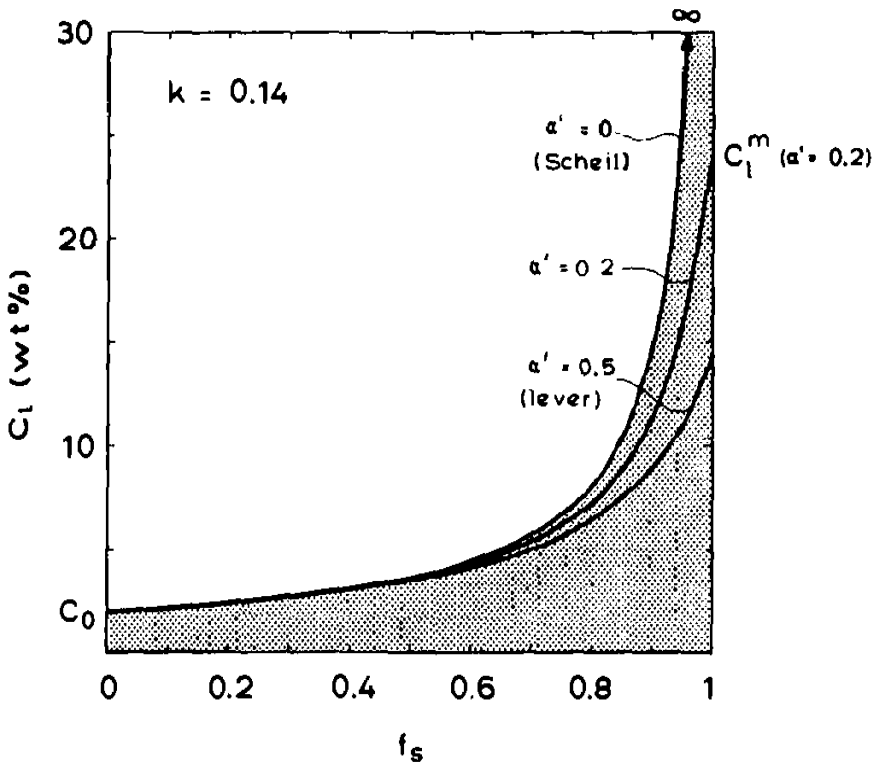

Figure 6.4: SEGREGATION CURVES IN THE PRESENCE OF BACK DIFFUSION. The composition of the liquid (assumed to be homogeneous as in figure 6.3) increases at the end of the specimen. Under lever-rule conditions, the increase is from C_0 to C_0/k, while the Scheil equation predicts an increase from C_0 to infinity. All of the intermediate cases can be described by one relationship (equation 6.9) which contains a modified α-parameter, α', which can take values between 0 and 0.5. Note that the curve represents the path of the interface concentration, C_l^*, as a function of f_s. The final solute distribution profile in the solid cannot be determined in this way because it changes with time when $\alpha > 0$. Therefore, only the end concentration ($f_s = 1$) represents a measurable value.

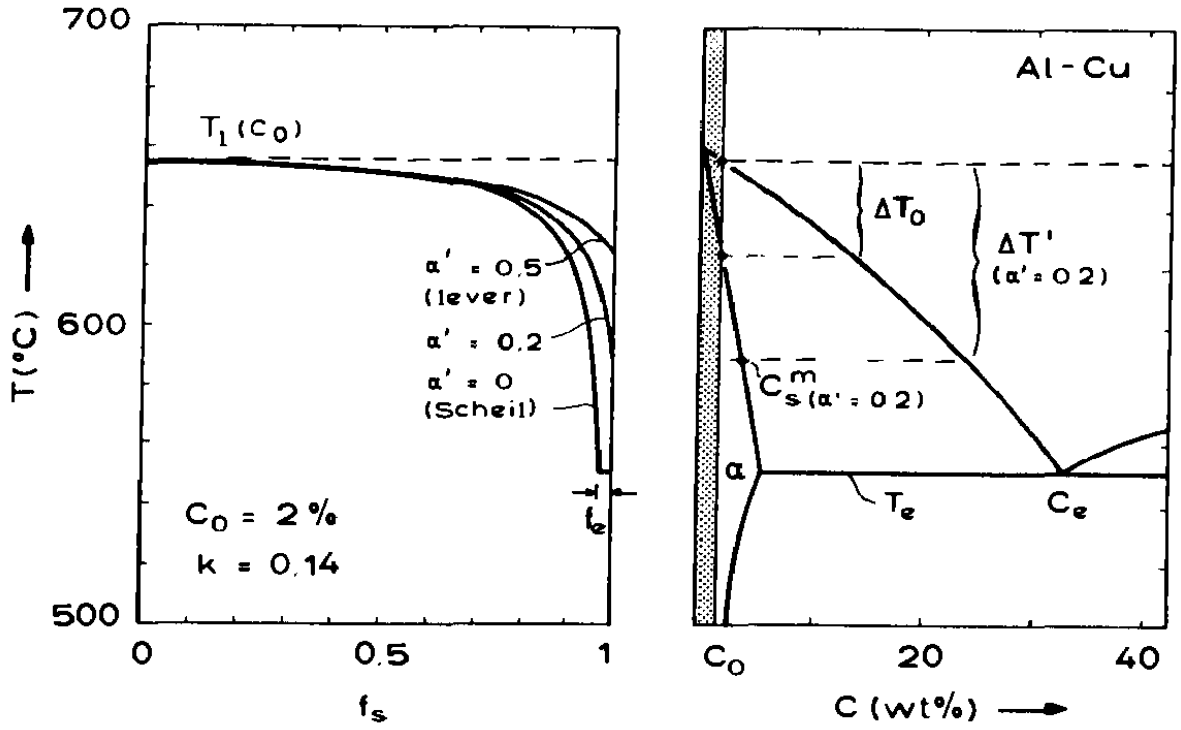

Figure 6.5: RELATIONSHIP OF THE SEGREGATE FREEZING POINT TO THE PHASE DIAGRAM. An increasing concentration (for distribution coefficients less than unity) is associated with a decreasing liquidus temperature since the slope, m, is then less than zero. Using the curves of figure 6.4, the temperature of the liquid as a function of volume fraction solidified can be derived. The use of realistic diffusion coefficients shows that, for small systems (such as interdendritic regions - figure 6.6) interstitial C in delta- and gamma-Fe will behave according to the lever-rule. Hence, the last liquid of a binary Fe-C melt will solidify at a temperature close to the solidus while substitutional alloys, such as Al-Cu, which typically have much smaller solid-state diffusion coefficients will usually contain eutectic material in the last (interdendritic) regions to solidify even when the overall composition is less than the solubility limit at T_e.

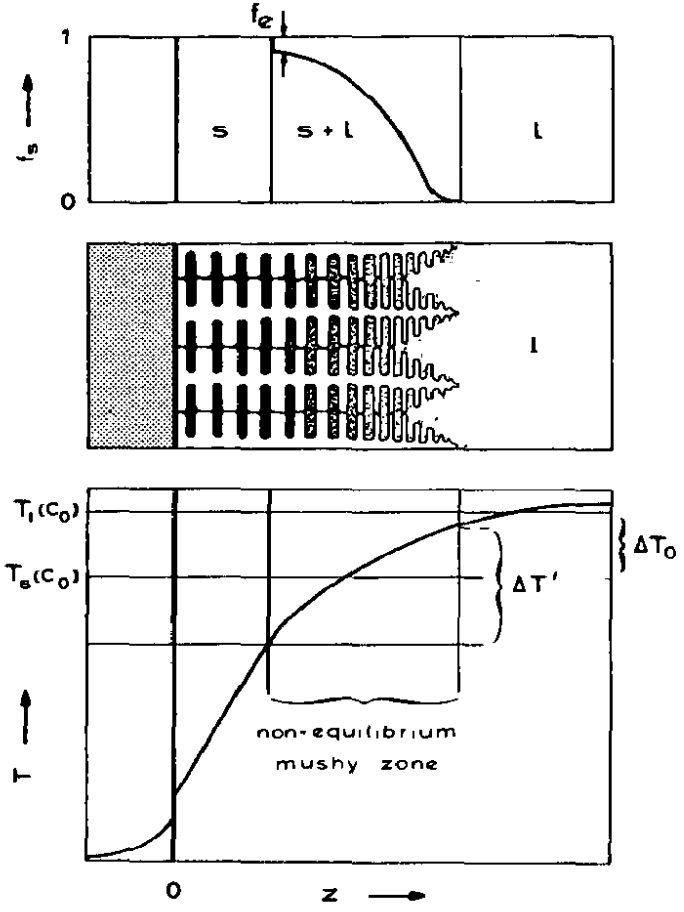

Figure 6.7: MICROSEGREGATION. The equilibrium melting range, ΔT_o does not, except for the lever rule case, correspond to the range, $\Delta T'$, over which the mushy zone develops. The dendrite tips need a certain undercooling which is determined by the stability of the tip. The dendrite roots will usually have much higher concentrations than C_o/k, due to non-equilibrium solidification. This often leads to interdendritic precipitation of eutectic phases of volume fraction, f_e, even if the composition is not on the eutectic tie-line. In the columnar zone of a casting, as shown here, the volume fraction of solid, f_s, will follow an S-shaped curve like that in the uppermost diagram.

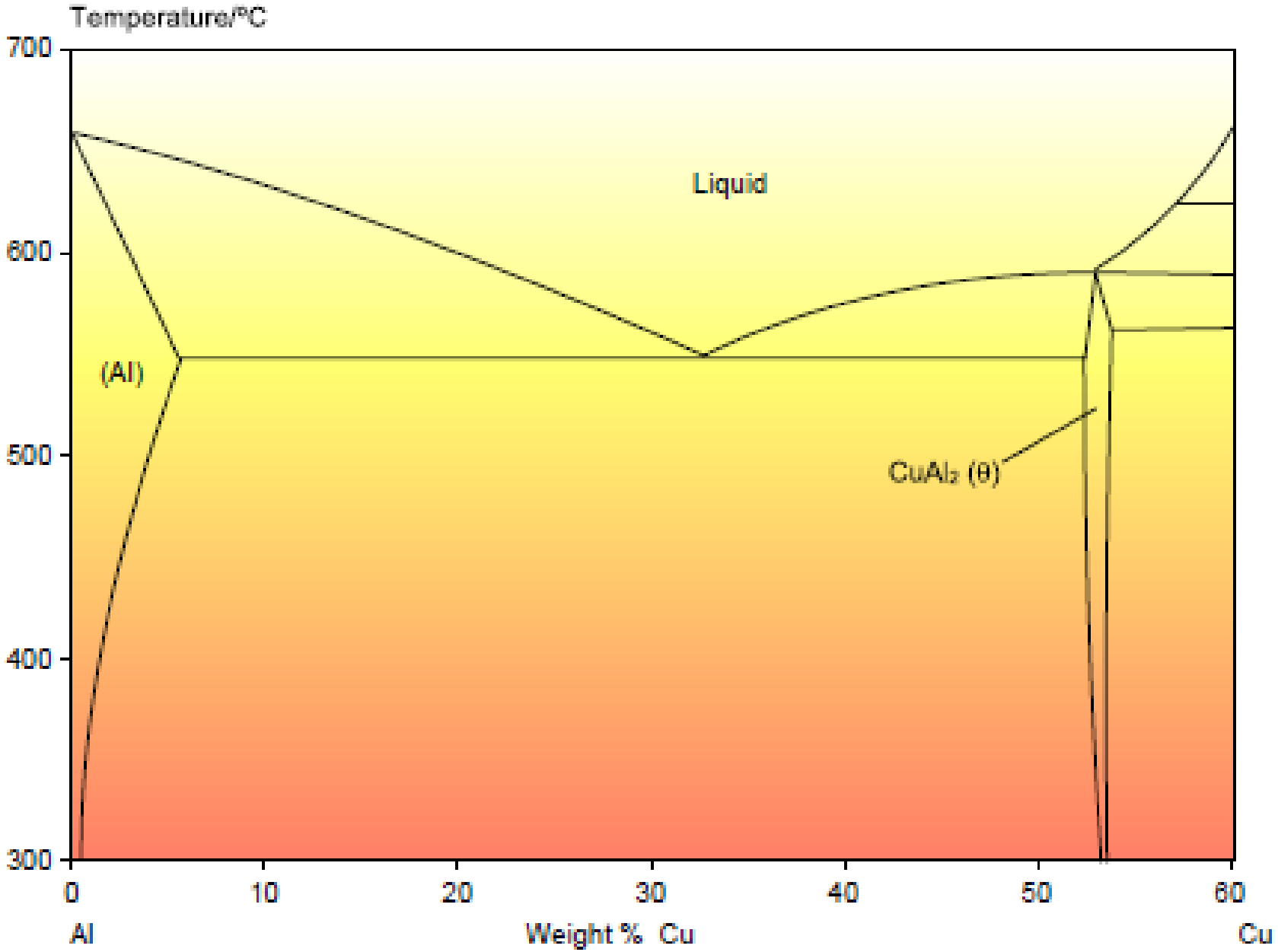
Temperature/°C
700
600
500
400
300
Liquid
(Al)
CuAl2 (θ)
0
10
20
30
40
50
60
Al
Weight % Cu
Cu

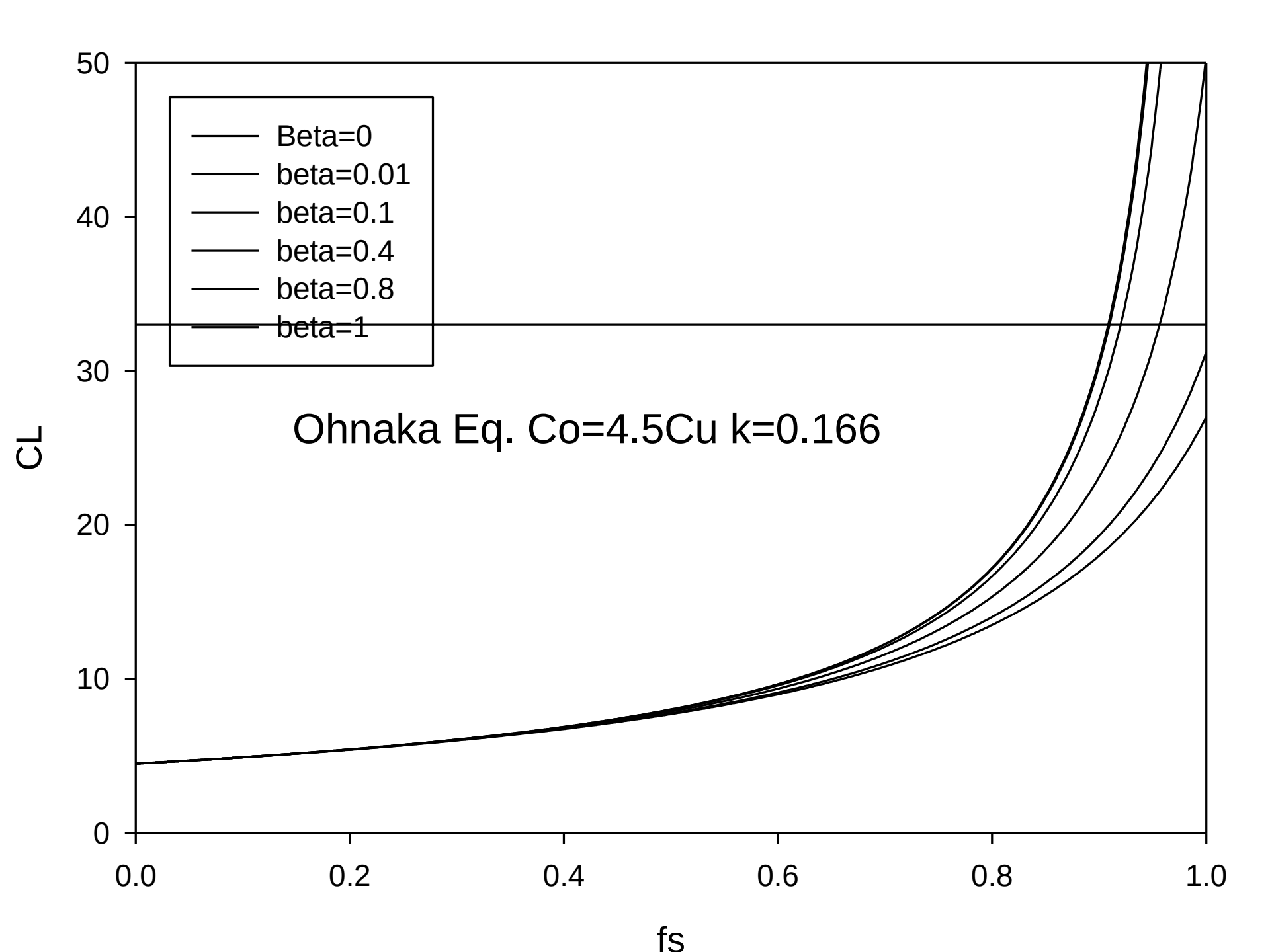
Beta=0
beta=0.01
beta=0.1
beta=0.4
beta=0.8
beta=1
Ohnaka Eq. Co=4.5Cu k=0.166
CL
fs
0
10
20
30
40
50
0.0
0.2
0.4
0.6
0.8
1.0

$$f_s = \frac{1}{1 - 2\alpha' k} \left[1 - \frac{T_f - T}{T_f - T_i} \right]^{\frac{1 - 2\alpha' k}{k - 1}}$$

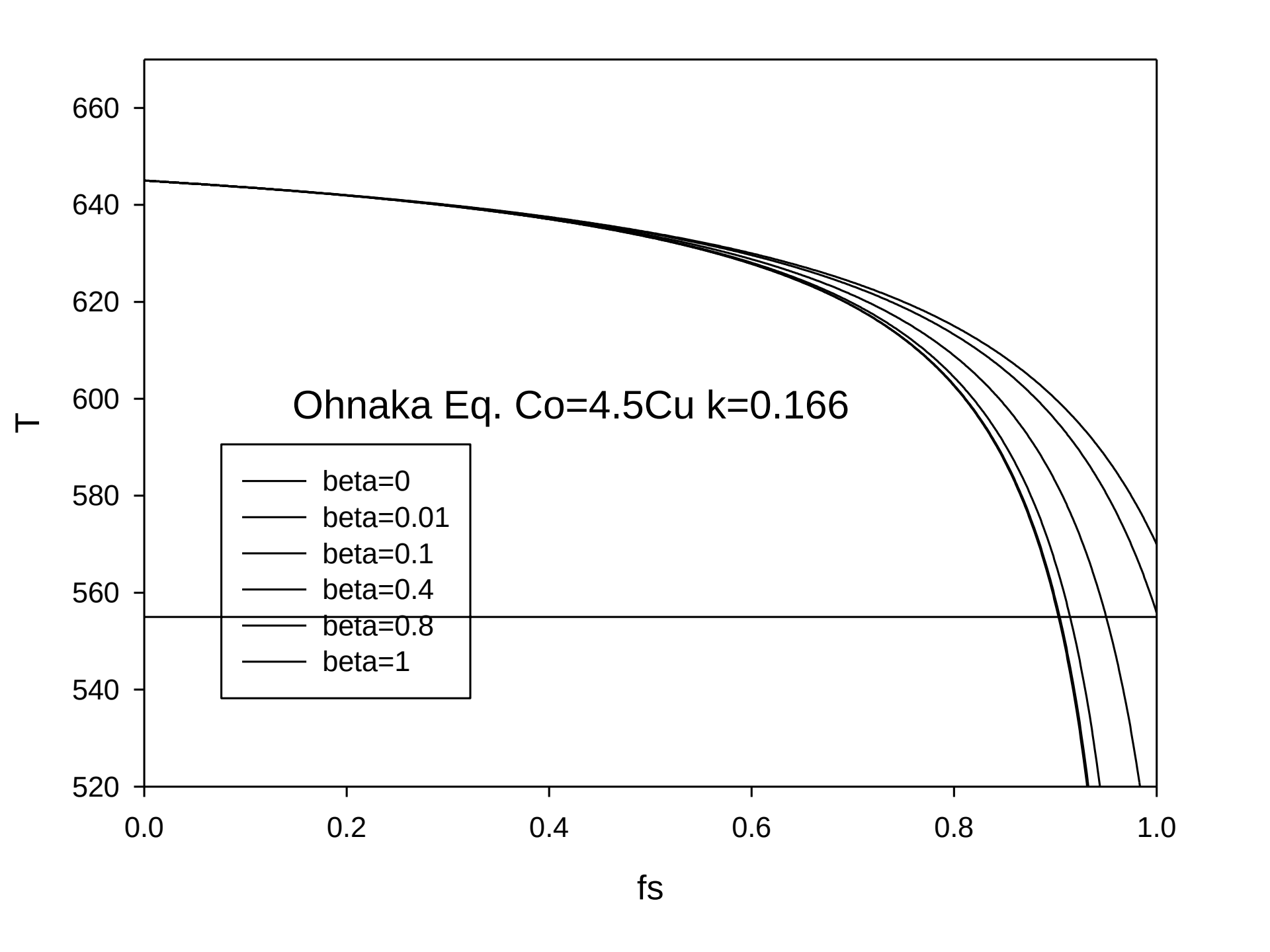
Ohnaka Eq. Co=4.5Cu k=0.166
beta=0
beta=0.01
beta=0.1
beta=0.4
beta=0.8
beta=1
T
fs
660
640
620
600
580
560
540
520
0.0
0.2
0.4
0.6
0.8
1.0

- 1 no mixing in liquid no diffusion in solid no coarsening
- 2. partial mixing in liquid no diffusion in solid no coarsening
- 3. complete mixing in liquid no diffusion in solid no coarsening
- 4. complete mixing in liquid diffusion in solid no coarsening
- **5. complete mixing in liquid diffusion in solid coarsening**
- 6. complete mixing in liquid complete diffusion in solid

The dimensionless parameter $\alpha=(D_S t_f)/L^2$ determines the extent of diffusion in the solid phase. Several authors criticized α dimensionless parameter for being not considered true back diffusion in solid, especially for rapid solid-state diffusion cases, $\alpha > 0.1$. For the parabolic growth rate, Clyne-Kurz replaced α parameter with Ω parameter which is also a function of α and but behave correctly over the whole range of α values for plate-like morphology [4].

$$\Omega(\alpha) = \alpha\left(1 - \exp\left(-\frac{1}{\alpha}\right)\right) - \frac{1}{2}\exp\left(-\frac{1}{2\alpha}\right). \quad (5)$$

Kirkwood modified the Brody-Flemings model for the dendrite arm coarsening situation [5]. He added the last term to the partial differential equation of Brody-Flemings This represents the

Beta=2*alpha/(1+2*alpha) Ohnaka

dilution of liquid due to the increase in the size of dendrite arm. In this model, the other assumptions are same as Brody-Flemings model.

$A_2=A_3+A_1+A_4$

$$(C_L - C_S)\frac{dx_i}{dt} = D_S\left(\frac{dC}{dx}\right)_{X_i} + (L - X_i)\frac{dC_L}{dt} + (C_L - C_O)\frac{dL}{dt}. \qquad (6)$$

$$C_S = kC_O\left(1-\frac{f_S}{1+b}\right)^{(k-1)} . \qquad (16)$$

Similarly, it can be easily shown that the analytical solution of Eq.6 for the parabolic growth rate becomes:

$$C_S = kC_O\left(1-f_S\left(\frac{1-2k\Omega}{1+b}\right)\right)^{\left(\frac{k-1}{1-2k\Omega}\right)} . \qquad (17)$$

M can be calculated by using a fitting program between the exact solution and this analytical model. For constant cooling, M is computed as a function of n and k by comparing the exact numerical model of Kirkwood [6] with Eq.16 whereas, for parabolic solid growth, M is obtained by comparing the Voller's parabolic solid growth model [7] with the Eq.16.

where $b = \frac{n}{M} = \frac{n}{\left(\frac{1.2+2.4n^{0.7}}{k}\right)}$. for constant cooling (18)

$$b = \frac{n}{M} = \frac{n}{\left(\frac{-41.12+51.59n^{0.12}}{k}\right)} . \quad \text{for solidification controlled by parabolic solid growth} \qquad (19)$$

M is constant and depends on partition coefficient, k, and coarsening exponent, n. It is also assumed that dendrite arms coarsen with time due to the power law equation:

$$L = At^n . \tag{8}$$

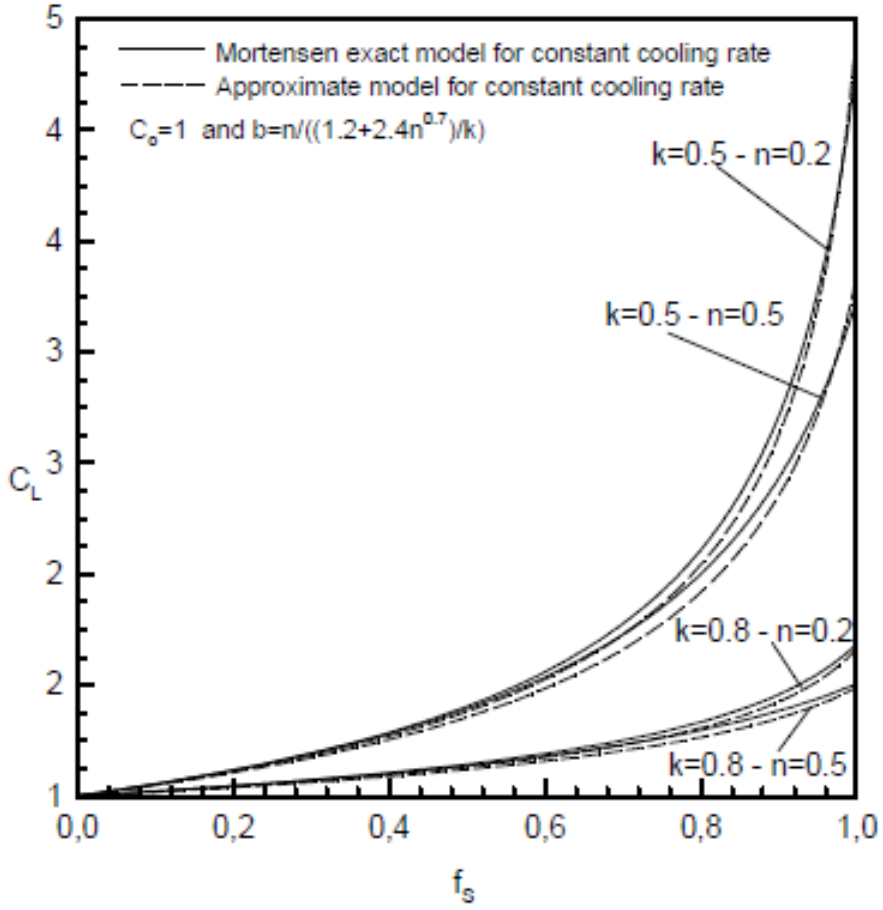

Figure 2 Comparisons between Mortensen exact model (solid line)[8] and approximate analytical model (dashed line) for constant cooling rate

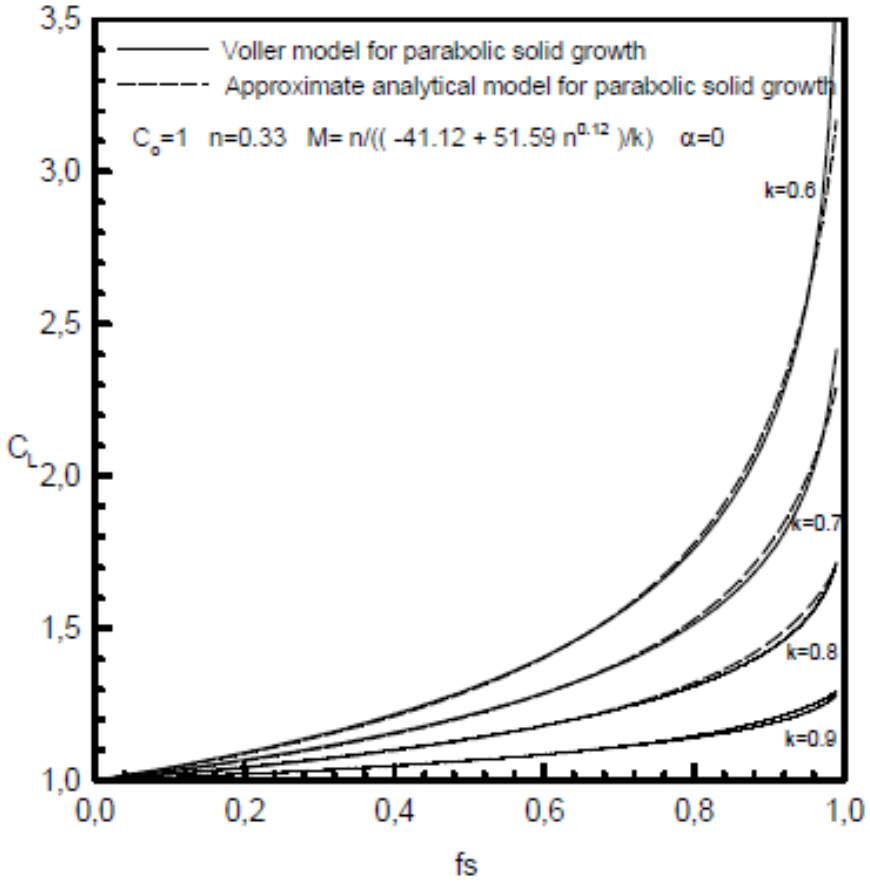

Figure 3 Comparisons between Voller model (solid line) and approximate analytical model (dashed line) for parabolic solid growth for different k values when α=0

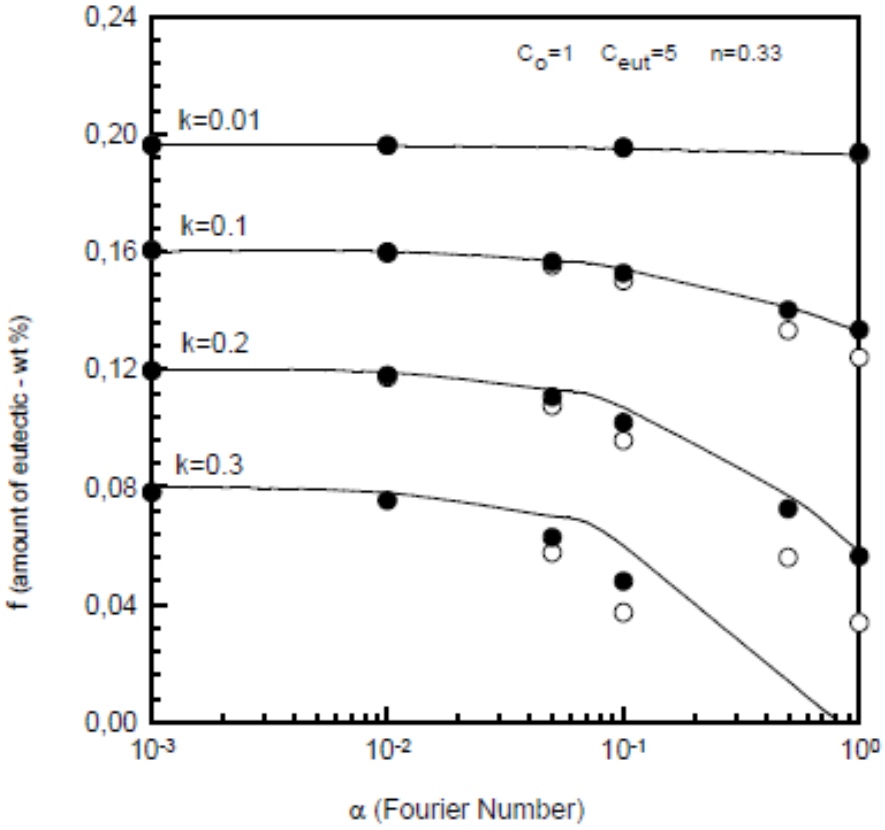

Figure 4 Comparisons between Voller's model (solid line) and approximate analytical model for parabolic solid growth for different k values as a function of Fourier number. (o for Ω and • for modified Ω, i.e. 0.75Ω)

Solidification in Ternary System

Solidification Path in Ternary Systems

In general, the path of solidification (trace of liquid or solid composition as a function of f_S) can be obtained in the case of solidification by relating the composition to f_l, which must be the same for all of the elements). Using equation A11.10 and A11.18:

$$\left(\frac{C_l}{C_o}\right)_B = (1 - u_B f_S)^{-\frac{p_B}{u_B}}$$

$$\left(\frac{C_l}{C_o}\right)_C = (1 - u_C f_S)^{-\frac{p_C}{u_C}} \qquad \text{[A11.25]}$$

where $u_i = 1-2\alpha_i' k_i$ and $p_i = 1-k_i$. Eliminating f_S:

$$\left(\frac{C_l}{C_o}\right)_B = \left\{1 - \frac{u_B}{u_C}\left[1 - \left(\frac{C_l}{C_o}\right)_C\right]^{-\frac{u_C}{p_C}}\right\}^{-\frac{p_B}{u_B}} \qquad \text{[A11.26]}$$

Solidification in Al-Cu-Mg Alloys

7050 Plate

Focus on one alloy (7050) and product (thick hot rolled plate)

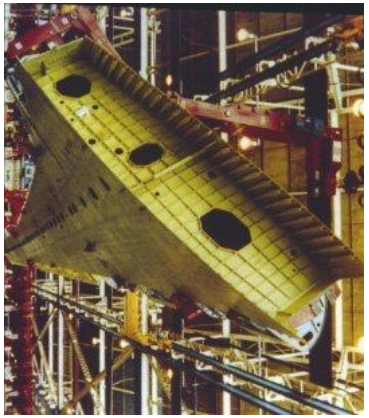

Components machined from 7050 alloy thick plate are widely used in load bearing applications e.g. wing spars

Si	Fe	Cu	Mg	Zn	Ti	Zr	Al
0.12max	0.15max	2.0-2.6	1.9-2.6	5.7-6.7	0.06	0.08-0.15	bal

7050 composition specification

Processing Sequence - 7050 Plate

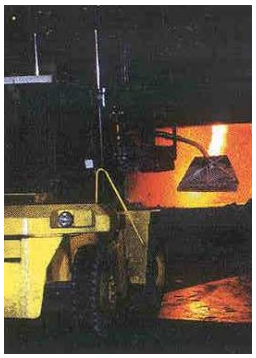

Cast
Direct chill

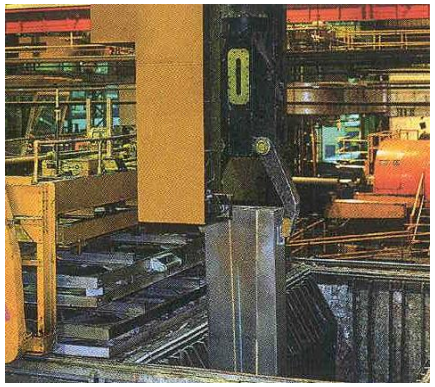

Homogenize
~475°C, 24h

Hot roll
~350-450°C
20+ passes
reduction~70%

Solution treat
475°C, 1h
spray quenched

Age

Microstructural Changes

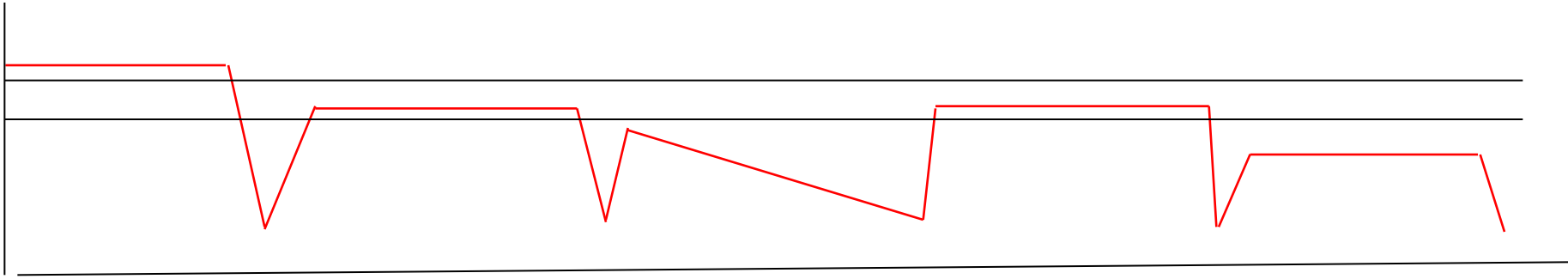

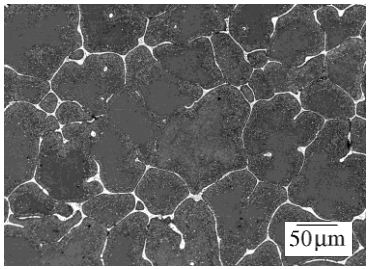

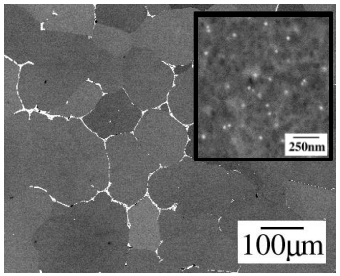

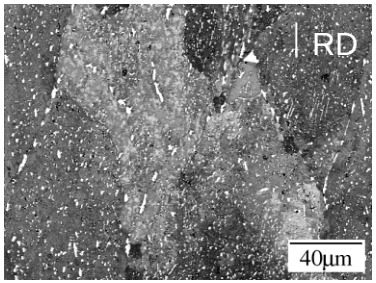

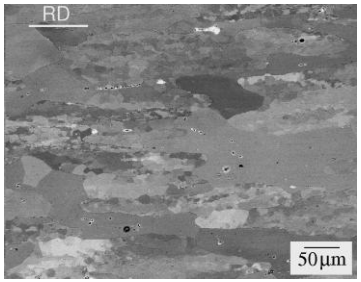

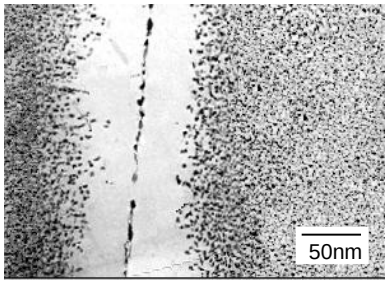

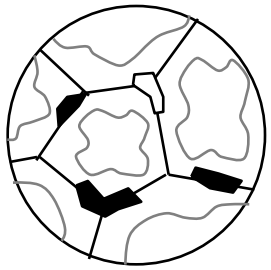

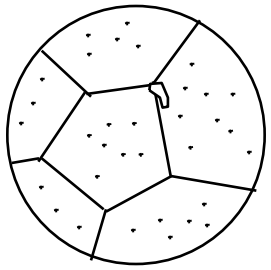

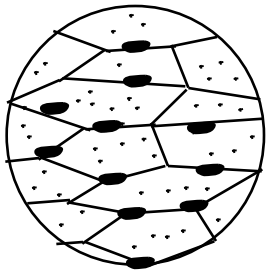

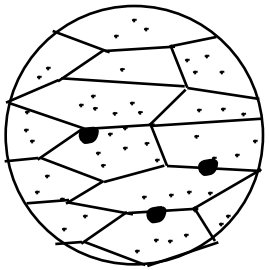

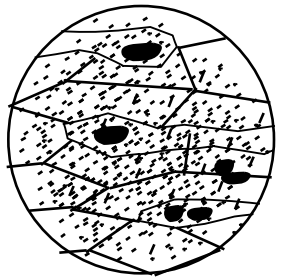

Cast Homogenized Rolled Solutionized Aged

Simple Phase Diagrams

Even for simple 2xxx alloy (Al-Cu-Mg), need data for 3 binaries and information about ternary phases

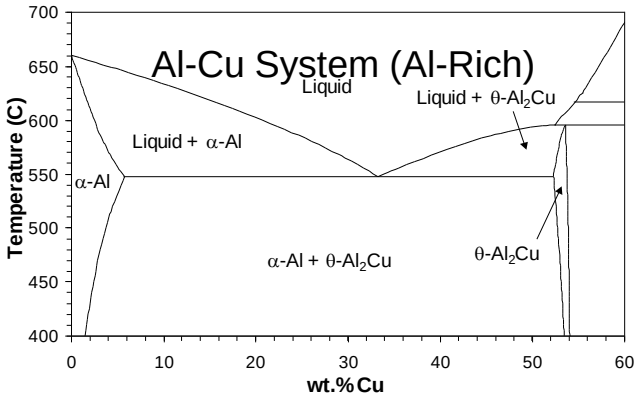

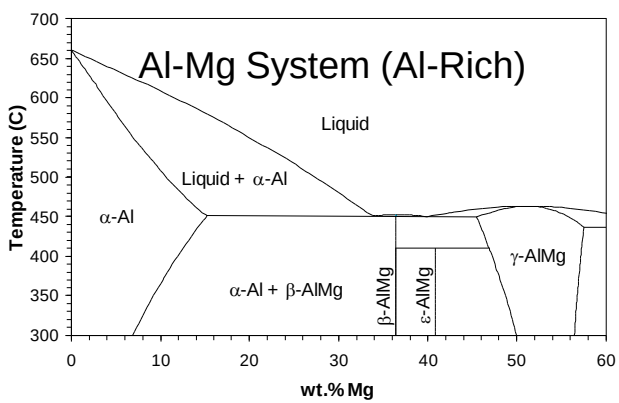

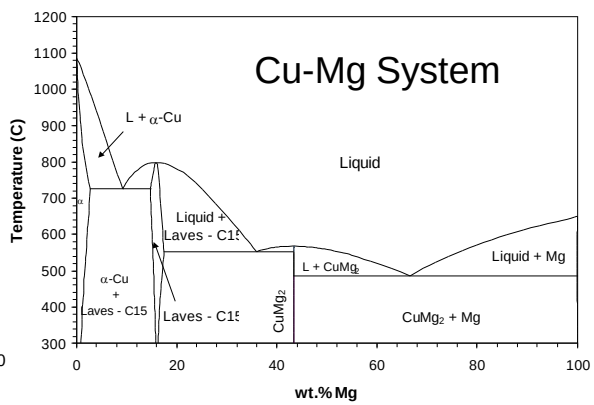

Ternary Phases S - Al_2CuMg, T - $Mg_{32}(Al,Cu)_{49}$, V - $Al_5Cu_6Mg_2$, Q - $Al_7Cu_3Mg_6$

MTDATA predicted phase diagrams

Real, commercial Al-alloys may contain > 10 alloying elements!

Success of thermodynamic models relies on availability of sufficient, high quality, thermodynamic data

Predictions for Binary Al-Cu Alloy

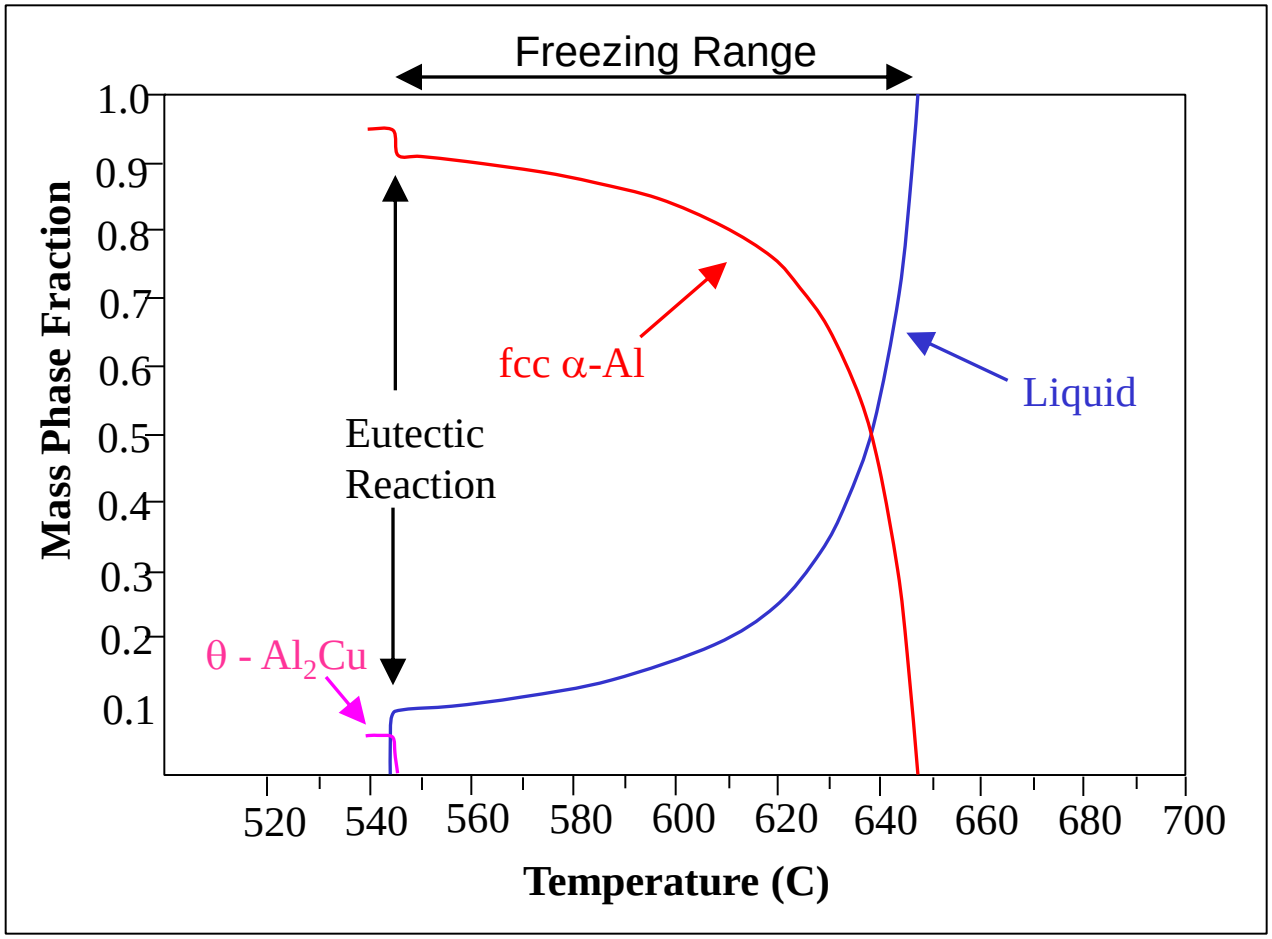

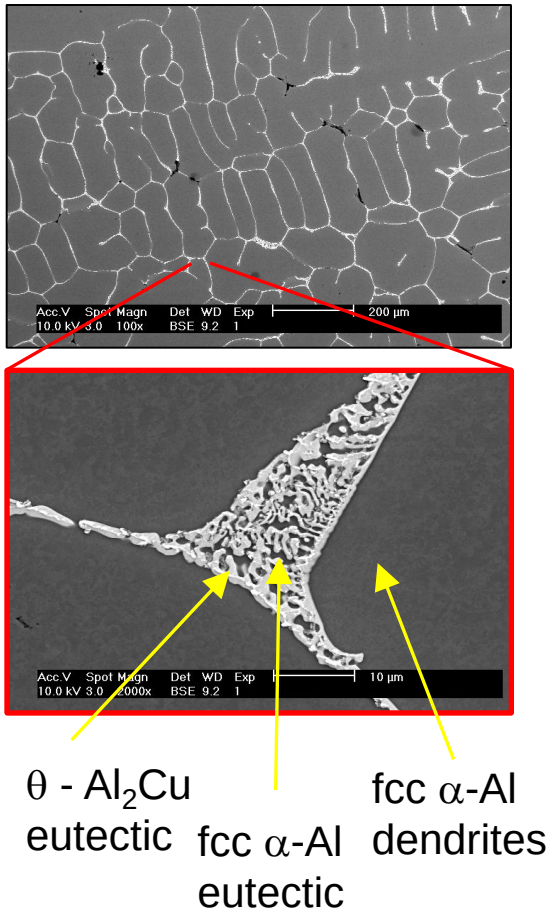

Predictions for Ternary Al-Cu-Mg alloy

Predictions for 2xxx (Al-4.5Cu-1.5wt%) Mg alloy

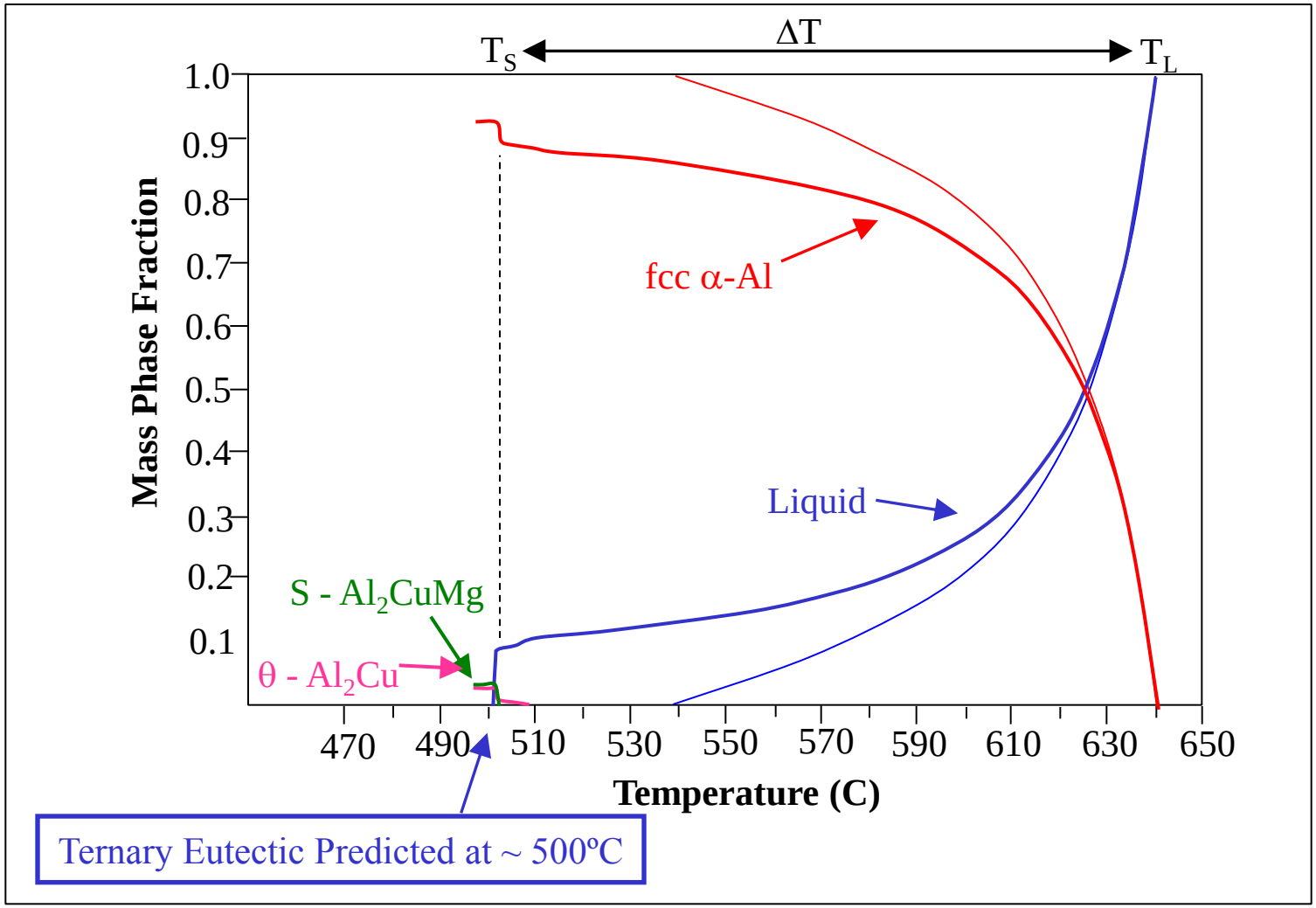

Prediction of Freezing Range

To reduce tendency for solidification cracking, need to minimize absolute freezing range

Use thermodynamic model to predict freezing range for different alloy compositions

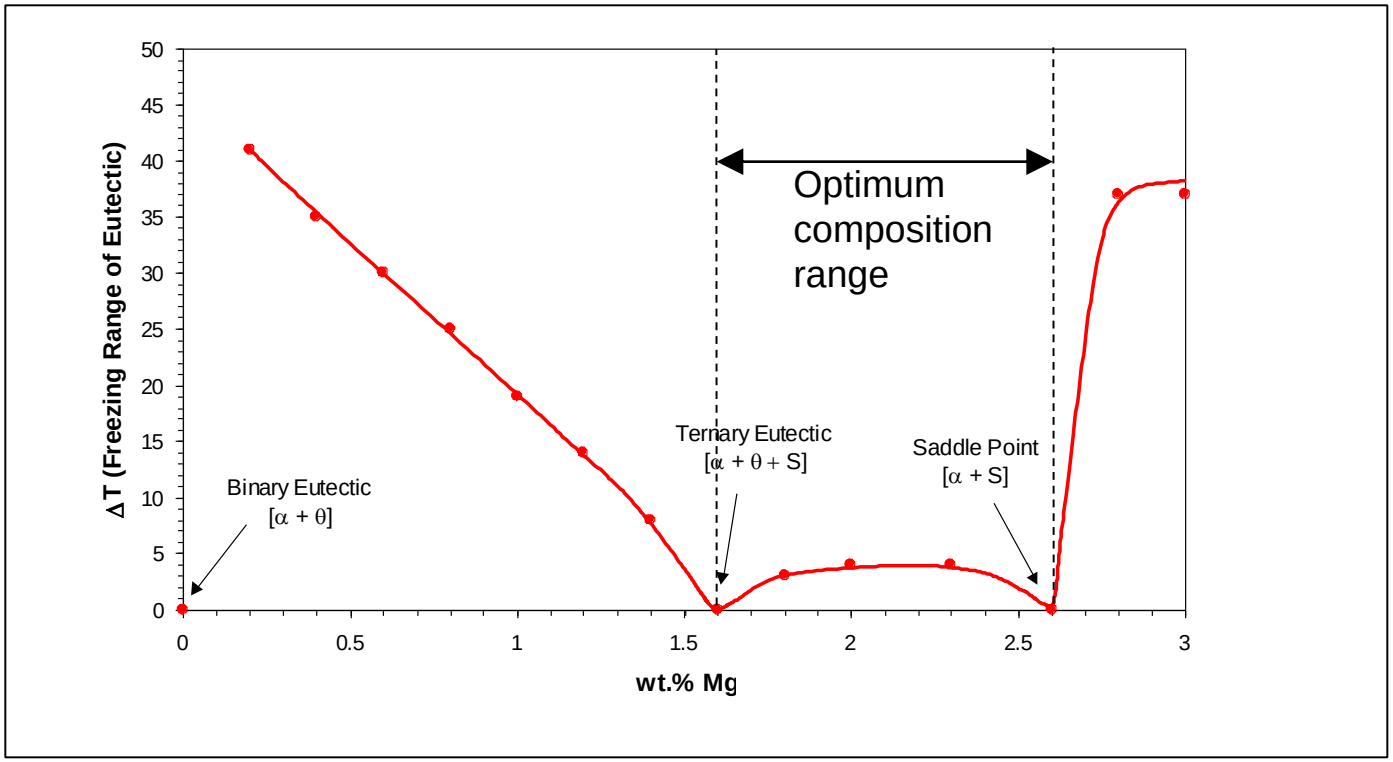

Effect of Mg content on freezing range of eutectic in Al-4.5Cu-x Mg alloy

(a)

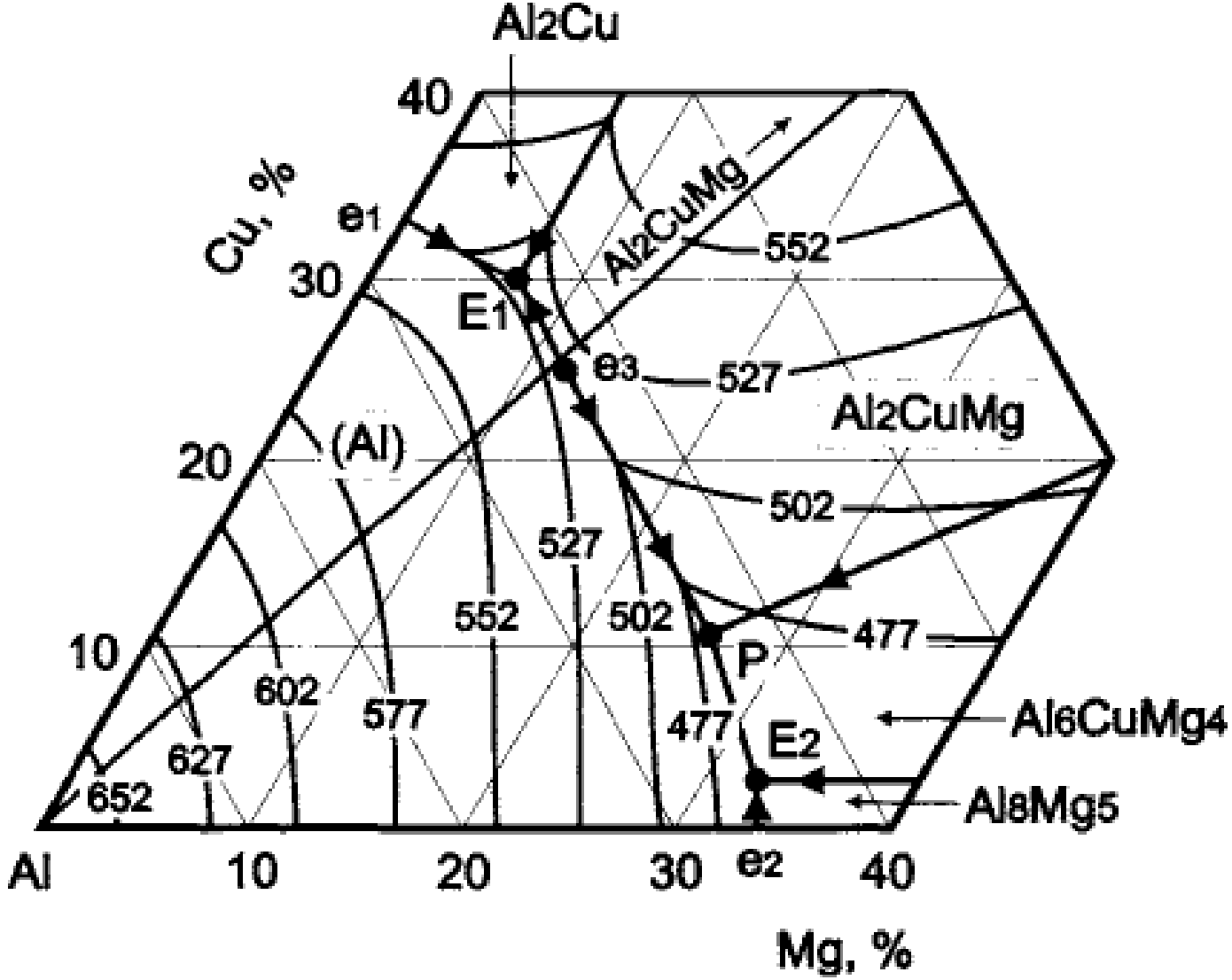
Al2Cu
40
Cu, %
e1
30
E1
Al2CuMg
552
e3
527
Al2CuMg
20
(Al)
502
527
552
502
10
477
P
602
577
477
E2
Al6CuMg4
627
652
Al8Mg5
Al
10
20
30
e2
40
Mg, %

Microsegregation in Manganese Steels

- Fe-C-Mn Aloys

Fe-C-Mn Phase Diagram

Table 1: Chemical Composition of the Investigated Steels.

Alloy No	%C	%Mn	%S	%P	%Other
1	0.10	1.57	0.003	0.005	<0.02
2	0.21	1.60	0.003	0.005	<0.02
3	0.40	1.58	0.003	0.005	<0.02
4	0.75	1.59	0.003	0.005	<0.02

Table 2: Temperature Gradients in the Calibration Specimen as a function of Growth Rate for Three Series.

Series	Growth Rate (mm/s)	Temperature Gradient (K/mm) in liquid	in liquid+solid
1	0.025	8.4	10.2
1	.1	5.5	9
1	0.25	4.8	7.4
1	0.5	3.5	6.5
2	0.025	10.7	12
2	.1	7.2	10.5
2	0.25	5.9	9
2	0.5	4.6	7.4
3	0.025	13.2	15.6
3	.1	9.8	11.3
3	0.25	7.6	9.2
3	0.5	6.9	8.3

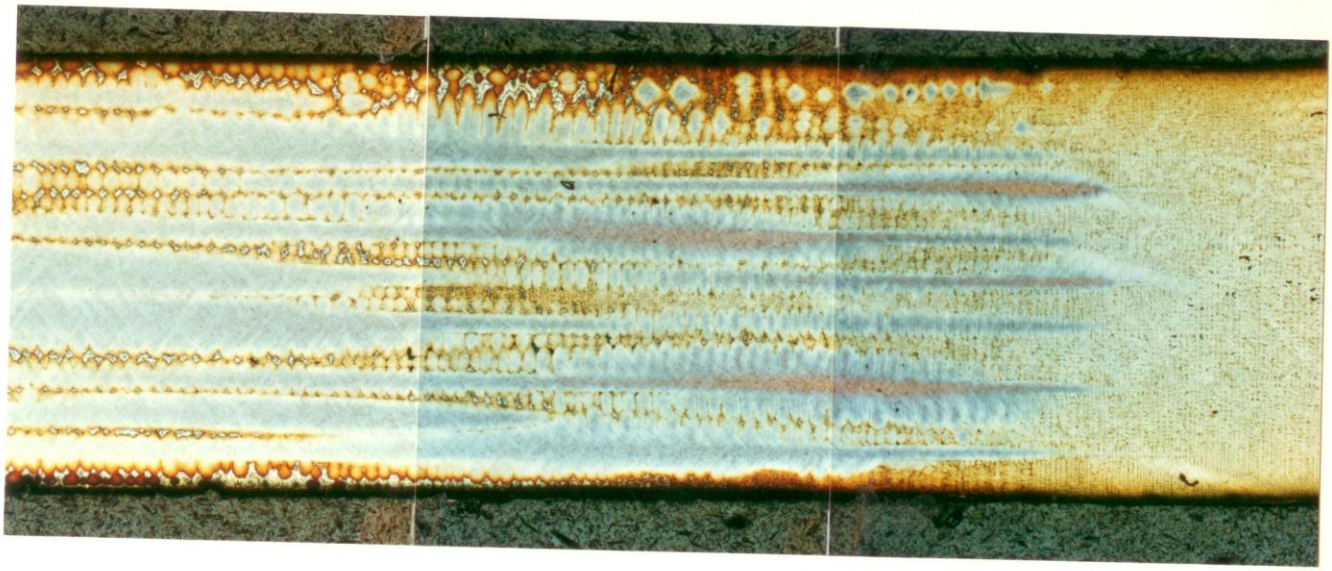

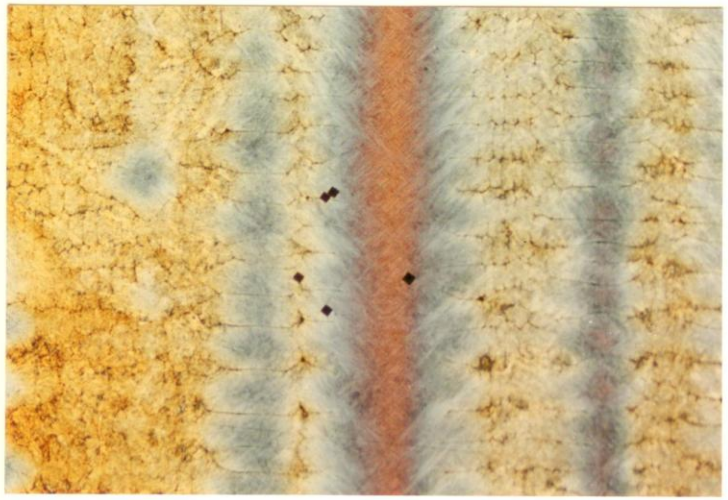

(a)

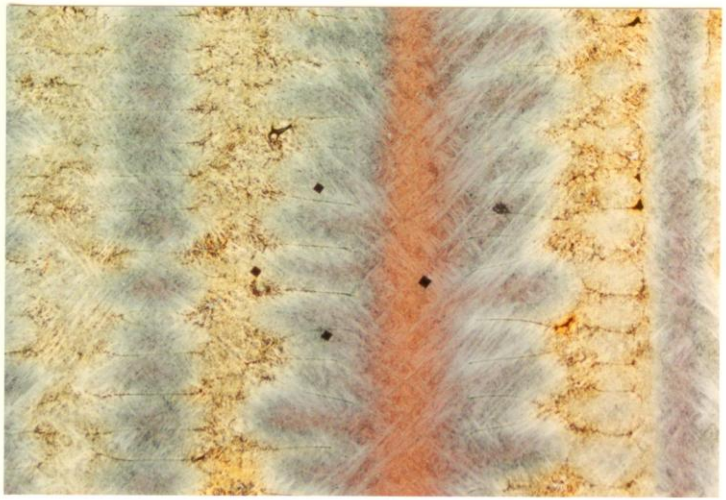

(b)

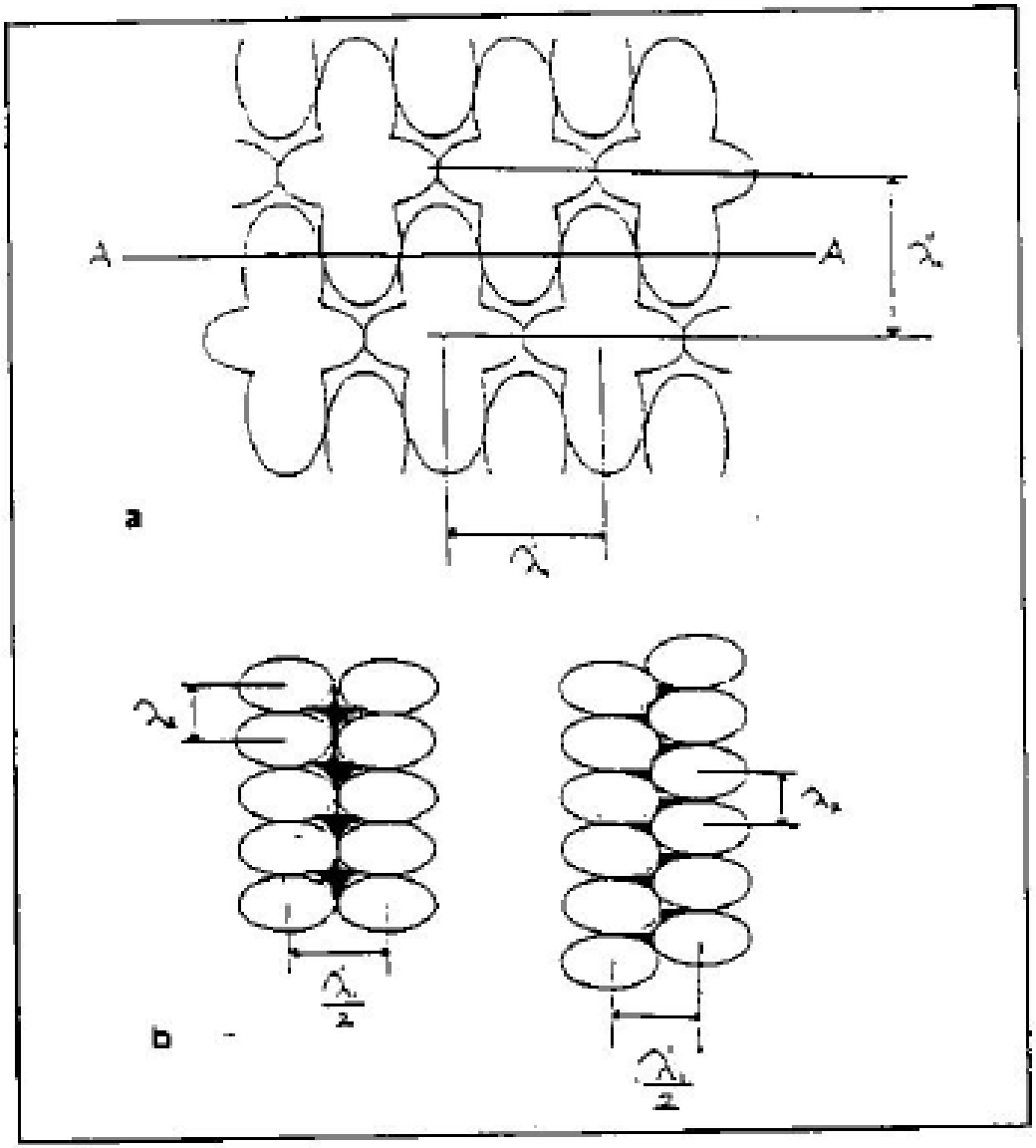

Figure 1: (a) The transverse section of close packed primary arm spacing arrangement. (b) The two extreme possible arrangement of secondary arms on the longitudinal section showing concave solidification model.

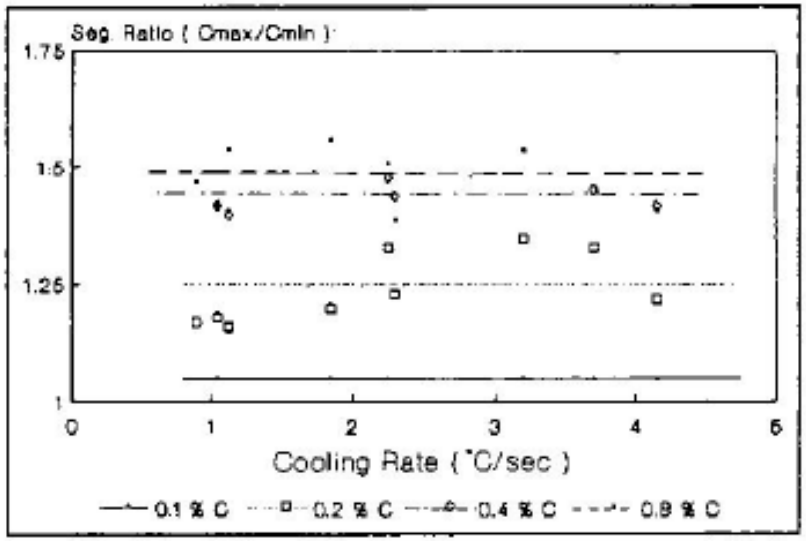

Figure 2: Segregation ratio between secondary arms as a function of cooling rate and carbon content at 1200°C.

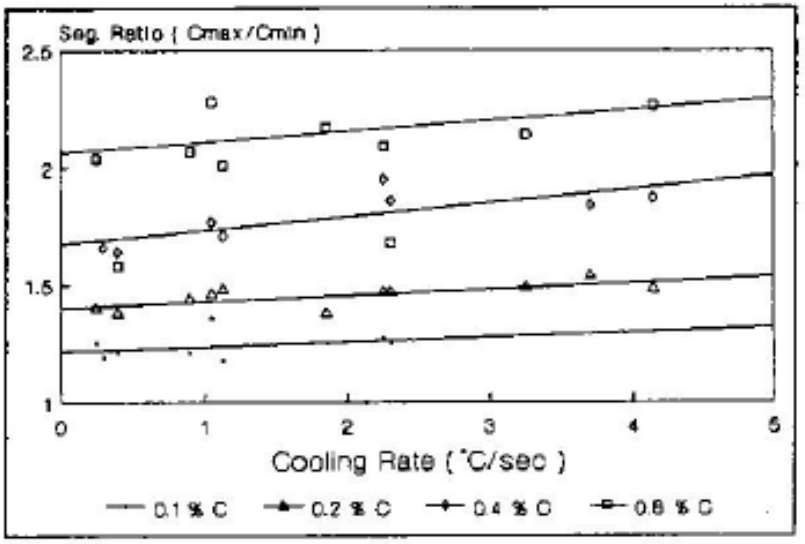

Figure 3: The segregation ratio of manganese as a function of cooling rate and carbon content at 1200°C.

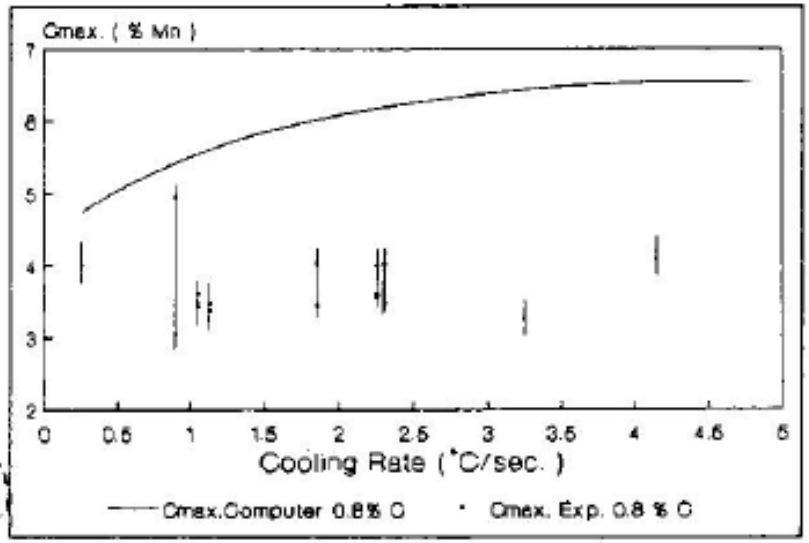

Figure 4: Comparison of predicted maximum concentration of manganese by concave computer model to the experimental results as a function of cooling rate at 1200°C (Fe–1.6%Mn–0.8%C)

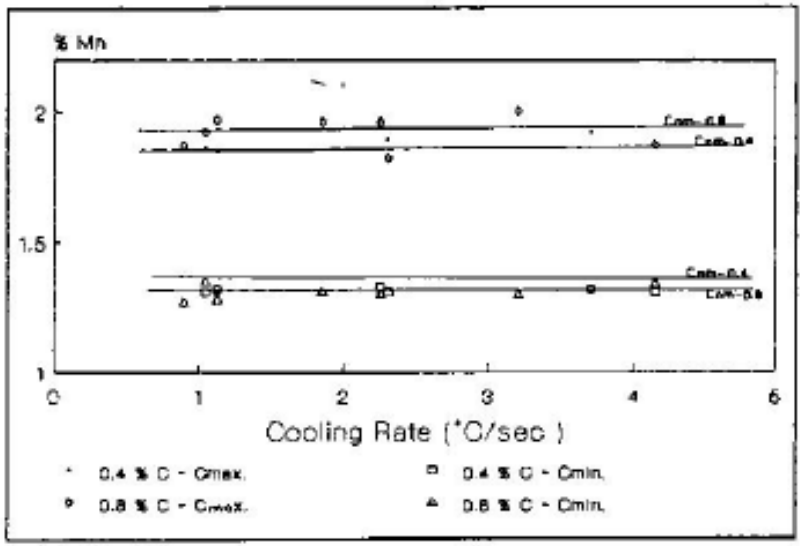

Figure 5: Comparison of predicted Cmax and Cmin of manganese by secondary arm coarsening model with the experimental results as a function of cooling rate for 0.4 and 0.8%C at 1200°C.

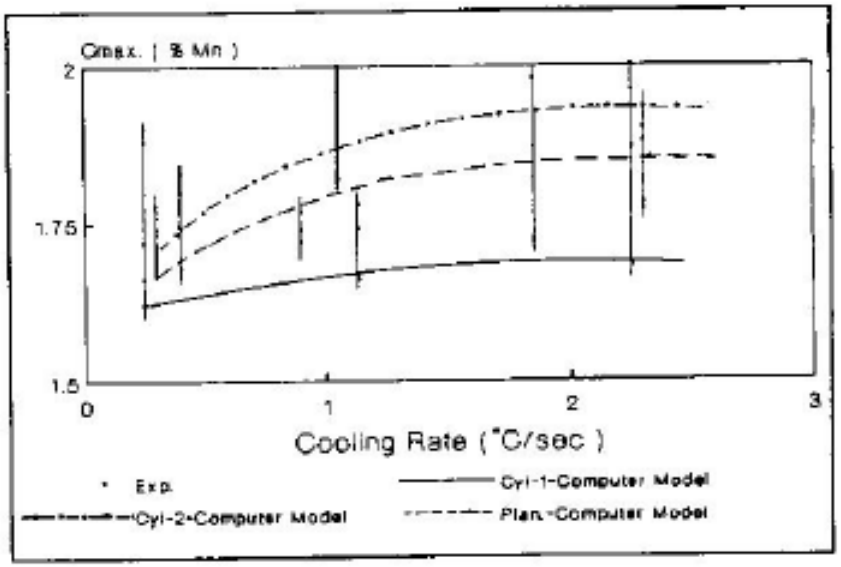

Figure 6: Variation of maximum concentration of manganese and computer results as a function of cooling rate for 0.1%C at 1485°C.

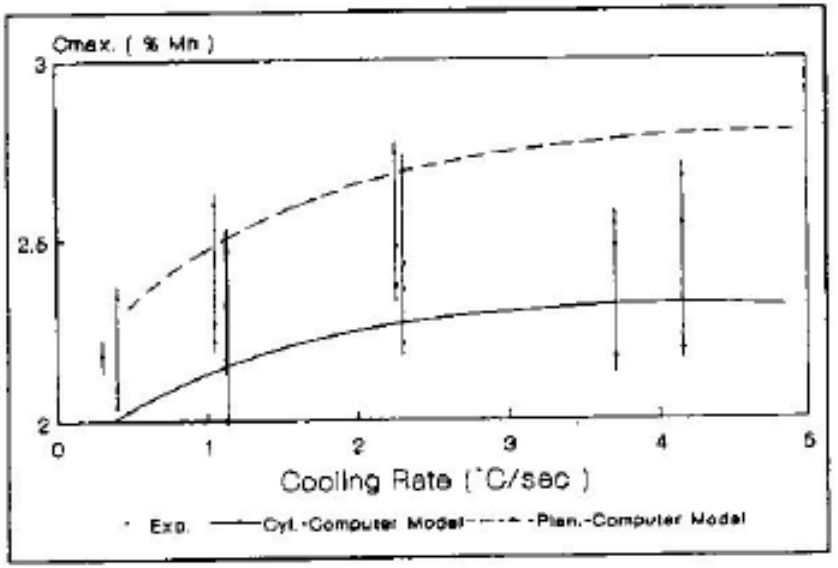

Figure 7: Variation of maximum concentration of manganese and computer results as a function of cooling rate for 0.4%C at 1200°C.

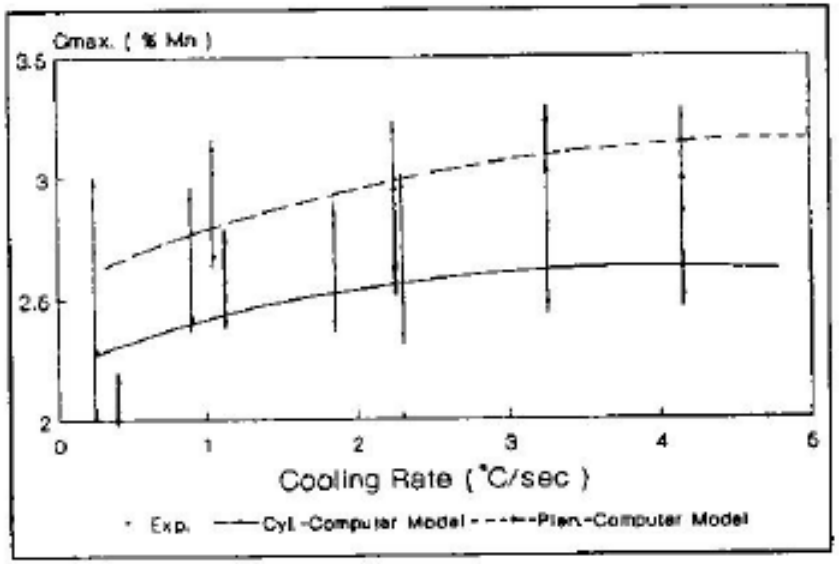

Figure 8: Variation of maximum concentration of manganese and computer results as a function of cooling rate for 0.8%C at 1200°C.

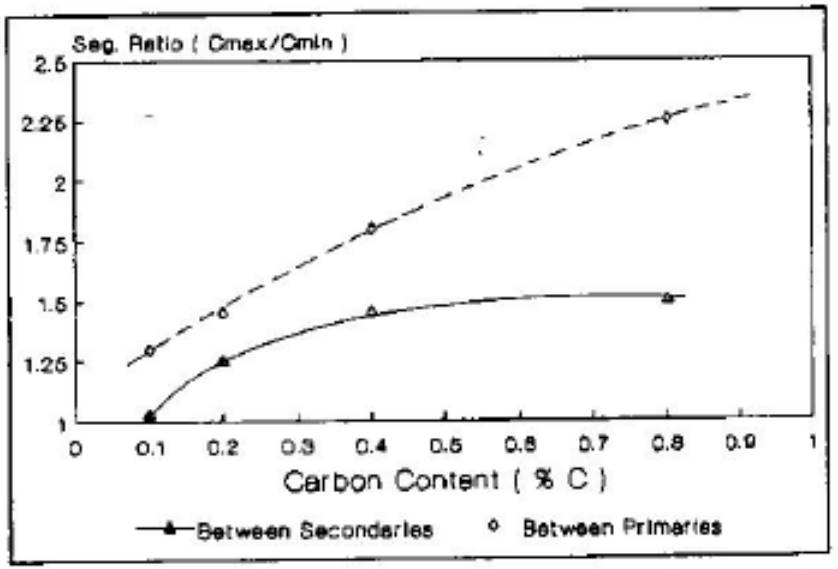

Figure 9: Average manganese segregation ratio as a function of carbon content for primary arms and secondary arms.

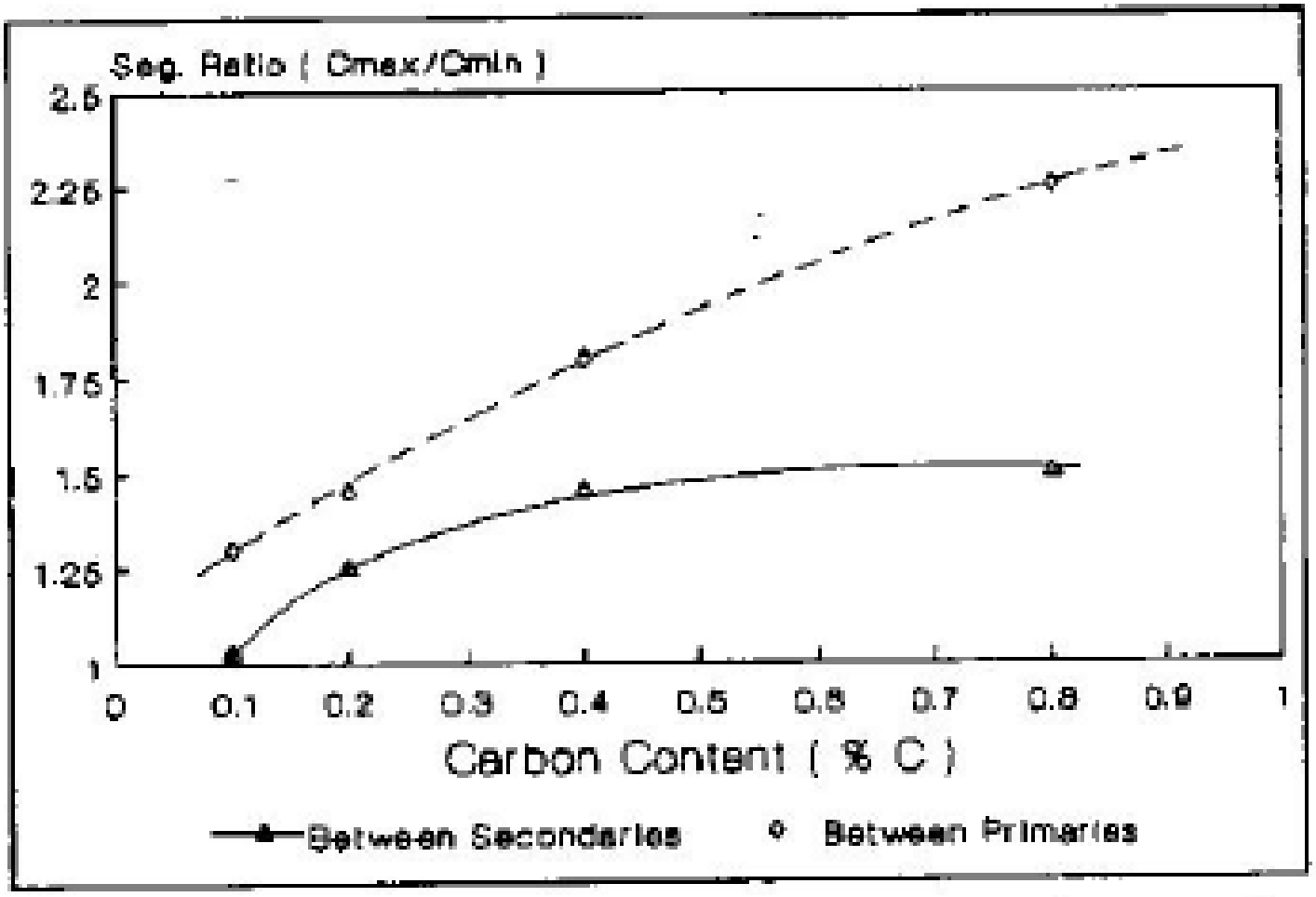

Figure 9: Average manganese segregation ratio as a function of carbon content for primary arms and secondary arms.

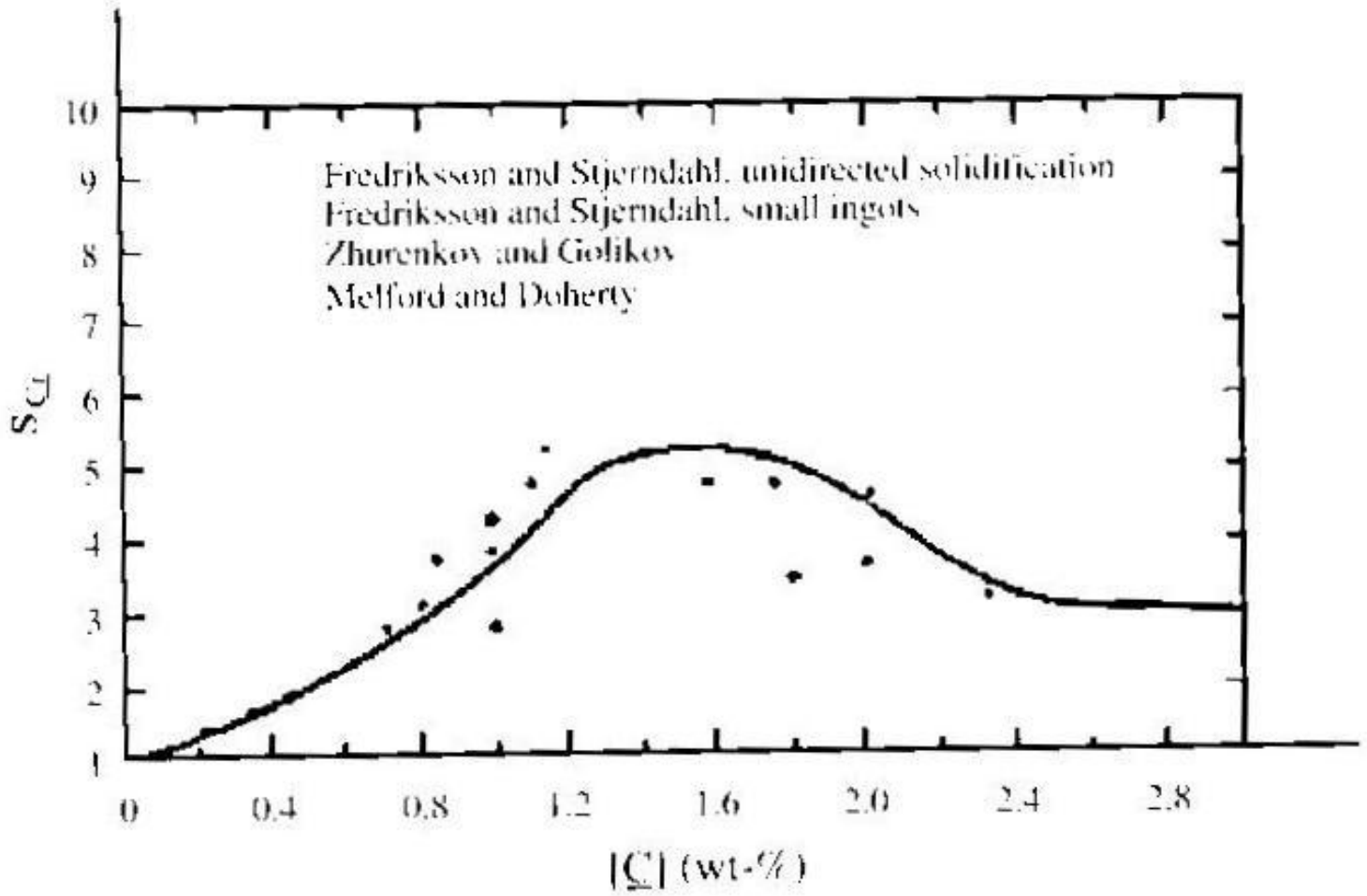

Figure 7.41 The degree of segregation of Cr as a function of the C concentration (in wt-%) in a series of Fe–Cr–C alloys with constant Cr concentration. The values, which are plotted in the diagram, originate from four different and independent investigations. Reproduced with permission from the Scandinavian Journal of Metallurgy, Blackwell.